

AN EXPERIMENTAL EVALUATION OF WIND TUNNEL WALL CORRECTION METHODS FOR HELICOPTER PERFORMANCE

Hans-Juergen Langer
 Deutsche Forschungsanstalt für Luft- und Raumfahrt e.V.
 Institut für Flugmechanik
 Braunschweig, Germany

Randall L. Peterson
 NASA Ames Research Center
 Moffett Field, CA

Thomas H. Maier
 Aeroflightdynamics Directorate
 Aviation Research, Development and Engineering Center
 U.S. Army Aviation and Troop Command
 Ames Research Center
 Moffett Field, CA

ABSTRACT

Accurate measurements of rotorcraft performance as measured in a wind tunnel are strongly influenced by the test section configuration, whether it be closed or open jet. The influence of wind tunnel walls on the induced velocity of lifting bodies has been studied by many researchers over the years. Methods have been developed to adjust the angle-of-attack and dynamic pressure for fixed wing aircraft in a wind tunnel to approximate free flight conditions. These methods have largely been adopted by the rotorcraft community with very little testing to verify the applicability of these methods to helicopter rotors and flight test measurements. Recent tests conducted by the Deutsche Forschungsanstalt für Luft- und Raumfahrt e.V. (DLR) in the Duits-Nederlandse Wind Tunnel (DNW) have provided data suitable for the evaluation of these methods. A 40% scale model Bo105 rotor was tested in five different wind tunnel test sections: 1) 6x6m closed, 2) 8x6m closed, 3) 8x6m open slots, 4) 9.5x9.5m closed, and 5) the 8x6m open jet. These data along with full-scale data from a NASA Ames 40- by 80-Foot Wind Tunnel test and a DLR flight test program provide a means to evaluate wind tunnel wall correction methods specifically for helicopter rotors. Good correlation of rotor power over a range of advance ratios for these three data sets has been shown using wall correction methods after accounting for trim deficiencies between the data sets.

Presented at the American Helicopter Society 52nd Annual Forum, Washington, D.C., June 4-6, 1996. Copyright © 1996 by the American Helicopter Society, Inc. All rights reserved.

NOMENCLATURE

a	two-dimensional lift-curve slope
A	area, m ²
c	blade chord, m
c _L	non-dimensional lift coefficient, wind axis
c _P , C _P	non-dimensional rotor power coefficient
c _T	non-dimensional thrust coefficient, shaft axis
<u>C</u>	rotor control vector
D	rotor diameter, m
<u>D</u>	derivative matrix
F	correction factor, Eq. (5)
F _X	x-force, N
F _Z	z-force, N
<u>F</u>	hub load vector (e.g., F _X M _Z)
L	lift, N
M _X	rolling moment, Nm

M_Y	pitching moment, Nm
M_Z	yaw moment or torque, Nm
p	per rev
R	rotor radius, m
s	rotor model-scale factor ($= 2.456$)
T	thrust, N
v_{tip}	rotor blade tip speed, m/s
V	tunnel speed or flight speed, m/s
W	test section width, m
Δc_{p_0}	profile power loss
Δc_{d_0}	profile drag loss
$\Delta\alpha$	rotor correction angle due to wall interference, rad or deg
α_s, α_{shaft}	rotor mast incidence, deg
δ_W	wall or boundary correction factor
$\theta_{0.7}$	collective pitch angle, $r/R = 0.7$
θ_c	lateral cyclic pitch angle
θ_s	longitudinal cyclic pitch angle
μ	advance ratio, V/v_{tip}
ρ	air density, Ns^2/m^4
σ	solidity

Abbreviations, Superscripts and Subscripts:

FS	full-scale
FT	flight test or free flight
Fus	fuselage
mo	model rotor
Re	Reynolds number

Ro	rotor
TPP	tip-path-plane
TS	test section
WT	wind tunnel

INTRODUCTION

The use of wind tunnel test measurements, flight test measurements, and analytical prediction plays a key role in the development of new rotor systems. Such tests are typically performed using a range of rotor system sizes and wind tunnel test facilities. To assure the accuracy of wind tunnel testing methodology, a validation study is in progress using test results from model- and full-scale tests in comparison with flight test data. This study is being conducted under the auspices of the U.S. Army/German Memorandum of Understanding on Cooperative Research in the Field of Helicopter Aeromechanics. This comparison will allow for a determination of the ability to accurately predict helicopter flight behavior from wind tunnel experiments and the influence of the test facility on these results. Experimental data from a series of wind tunnel tests, including both model- and full-scale experiments, have been studied to determine the extent to which wind tunnel test results can be used to predict flight behavior.

This paper presents the results of a recently completed model-scale test of a Bo105 hingeless rotor in the DNW. A 40% scale model Bo105 rotor ($R = 2.0m$) was tested in five different test sections of the DNW wind tunnel with the intent to evaluate and identify the influence of wind tunnel walls on measured rotor performance. The five different wind tunnel test sections used in this series of tests included the: 1) 6x6m closed, 2) 8x6m closed, 3) 8x6m open slots, 4) 9.5x9.5m closed, and 5) the 8x6m open jet. The influence of wind tunnel walls and the flow breakdown phenomenon has been studied and reported by many researchers over the years (Refs. 1-13). From these studies, a number of methods have been developed to account for tunnel wall induced effects in order to approximate free-flight conditions in the wind tunnel. Results from the DNW model-scale test were used to evaluate the applicability of two of these methods as they apply to rotorcraft testing. Additionally, the DNW data are compared with full-scale ($R = 4.912m$) data from a NASA Ames 40- by 80-Foot Wind Tunnel test (Ref. 14) and a DLR flight test program (Ref. 15) to further evaluate the wind tunnel wall correction methods.

TEST PROGRAM

Many wind tunnel tests are conducted with scaled models with the intention of determining the characteristics of full-scale flight aircraft. This is done to reduce costs and to obtain experimental measurements within a reasonable amount of time. There is, however, a great leap between a small-scale wind tunnel test and a full-scale flying vehicle. Differences in structure, rotor trim, rotor/body interaction, and the like may cause the scale model test to not be representative of the full-scale aircraft. Investigations into improving wind tunnel testing methodologies and evaluation of the suitability of scaled model testing to determine full-scale flight characteristics are the main goals for the rotor data correlation task within the Memorandum of Understanding (MOU) between U.S. Army/NASA and the Institute of Flight Mechanics of "Deutsche Forschungsanstalt für Luft- und Raumfahrt" (DLR). Correlation efforts have been conducted, based on flight tests, NASA Ames 40- by 80-Foot Wind Tunnel tests with a full-scale Bo105 rotor and a test program with a scaled Bo105 rotor/fuselage in the German-Dutch wind tunnel (DNW). Representative photos of each of the test programs are shown in Fig. 1.

Flight Test Program

The primary task of the flight test program was to provide the basis for follow-on wind tunnel tests of a full-scale rotor in the NASA Ames 40- by 80-Foot Wind Tunnel and a model-scale rotor in the German-Dutch wind tunnel. For the data correlation task, flight data acquired at a density altitude of approximately 762 m (2500 ft) was used. Steady-state flights were performed between hover and the maximum speed of the helicopter, with a stepsize in speed of approximately 10 knots.

The primary task of the test pilot was to establish a steady-state condition with minimum climb/descent, sideslip or pitch rate for each forward speed. Once the pilot was 'on condition' data was acquired with hands off the controls. Unfortunately, when gathering data with the pilots hands off the controls the aircraft maintains a steady level flight condition for a very short period of time due to the aircraft's instability. For this reason only the first three rotor revolutions were processed to form the flight test database. Each speed sweep was repeated three times to assess data scatter.

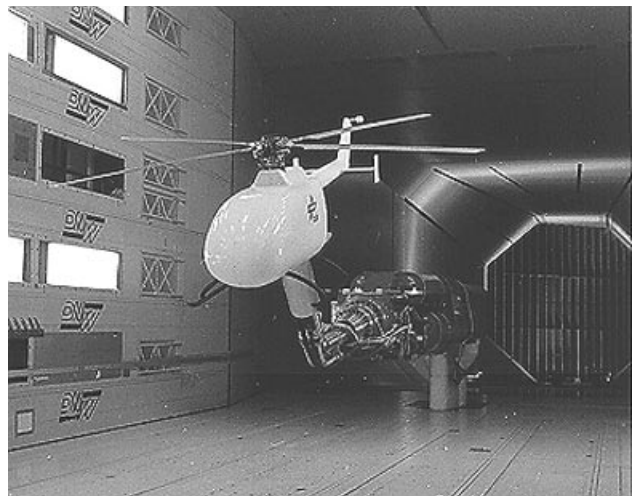
Rotor thrust could not be measured directly in the flight test program, therefore, the aircraft weight was used as an approximate measure. Weight was also not a direct measure, therefore the helicopter was weighed before and after each flight, and it was assumed that fuel



a) flight test



b) full-scale rotor



c) model-scale rotor

Figure 1. Test programs; a) flight test of Bo105 Helicopter b) full-scale tests in the 40- by 80-Foot Wind Tunnel and c) model-scale tests in the DNW.

consumption was linear with time as shown in Fig. 2. To minimize the influence of this approximation on aircraft weight, the flight tests were performed as quickly as possible. It was found from the analysis of the data that the flight test data presented in this paper is valid for a $c_T = 0.005 \pm 0.0001$.

Since the data correlation program in the various wind tunnels is primarily based on flight test data, emphasis was placed on the creation of a reliable data base. This data base consists of different sensors signals, some of which are used just to confirm the validity of other sensors. For example, the rotor mast torque was used to determine rotor power, while the power indication from the cockpit was used to check the mast torque as shown in Fig. 3.

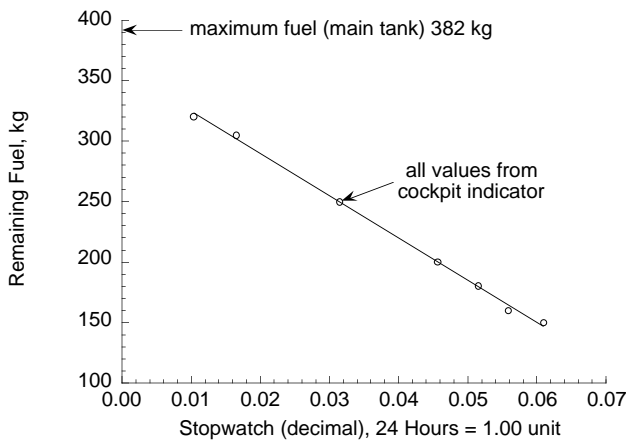


Figure 2. Flight test fuel consumption as a function of time.

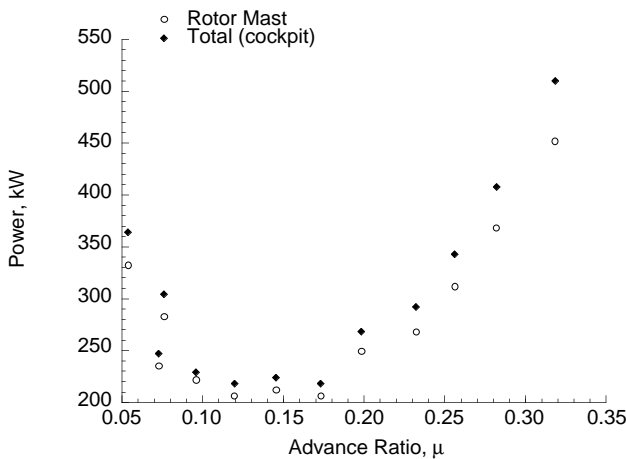


Figure 3. Accuracy check of rotor mast power sensor using the total power indicator from cockpit.

The total power data shown in Fig. 3 includes the tail rotor power, the gearbox efficiency, and the generator power. The power measurements shown in Fig. 3 in the low speed region, for $\mu < 0.1$, suggest that the speed indicator does not provide an accurate measure in this region. Both measures of power track with one another well, but the curve with speed is not smooth. In this low speed region the airspeed sensor is probably adversely influenced by the rotor downwash.

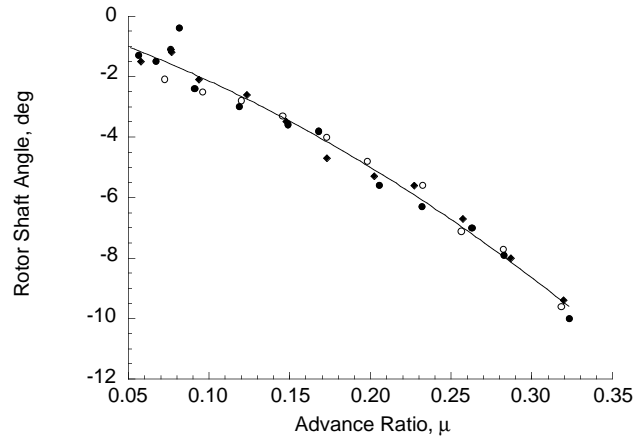


Figure 4. Shaft angle versus advance ratio for three test runs at constant density altitude.

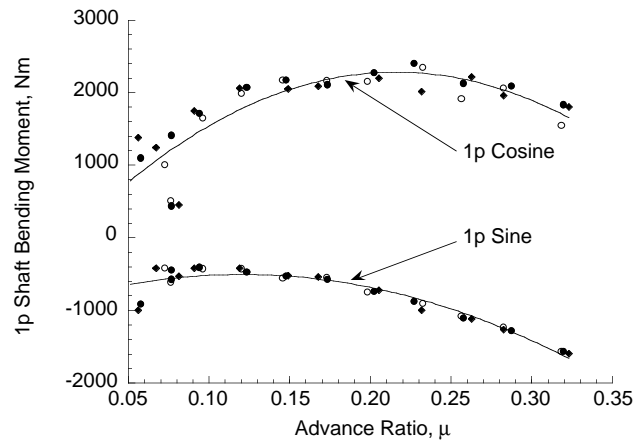


Figure 5. Mast bending moment versus advance ratio for three test runs at constant density altitude. The 1p cosine moment is the pitching moment and the 1p sine moment is the rolling moment.

Other important sensors for the correlation of flight and wind tunnel data are the rotor shaft angle (or fuselage attitude) and the mast bending. Figure 4 shows the shaft angle measurement versus advance ratio for three different

speed sweeps. Repeatability of the shaft angle measurement as compared with the least-squares curve-fit shows acceptable data scatter. Hub pitch and roll moments were determined from the rotating shaft bending gauges. A once per revolution spike over the tail of the aircraft provided a phase reference. The shaft bending moments were harmonically analyzed and the 1p cosine and 1p sine values were taken as the steady pitch and steady roll moments, respectively. These measurements may be seen in Fig. 5 for three speed sweeps. Again, the repeatability is acceptable.

Figures 4-5 provided the basis for trim settings in the wind tunnel test programs in the NASA Ames 40- by 80-Foot Wind Tunnel and in the DNW.

Other important parameters that were measured include rotor rpm, temperature, and pressure. In addition, a single blade was highly instrumented with 16 strain gauges. The flapwise strain gauges, 11 in all, provide a means to assess the elastic bending portion of the rotor tip path-plane. The large number of sensors along the blade span allows for the determination of the higher blade bending modes and allows for the evaluation of the location and number of sensors necessary to find these modes. The rotor was also instrumented with four lead-lag and one torsion sensor.

NASA Ames 40- by 80-Foot Wind Tunnel Tests

From the results of the flight test program, wind tunnel tests were conducted in the NASA Ames 40- by 80-Foot Wind Tunnel test section with a full-scale Bo105 Rotor installed on the NASA Ames Rotor Test Apparatus (RTA) as shown in Fig. 1b. Reference 15 describes this test program and presents the correlation of these results with flight test.

The RTA is a special-purpose drive and support system for operating helicopter rotors in the 40- by 80- and 80- by 120-Foot Wind Tunnels. The RTA houses two electric drive motors, the hydraulic servo-actuators of the primary control-system, and a dynamic control system capable of introducing dynamic perturbations to the non-rotating swashplate (collective and tilt) at frequencies up to 40 Hz. Installed on the RTA is a five-component steady/dynamic rotor balance to determine rotor loads at the hub moment center. The balance was designed and fabricated to measure both the steady and vibratory rotor normal, axial and side forces, together with rotor pitching and rolling moments up to rotor thrust levels of 98,000 N (22,000 lb). An instrumented flex-coupling measures rotor torque and the residual normal force.

Instrumentation for the 40- by 80-Foot Wind Tunnel test included the five-component rotor balance and instrumented flex-coupling, thirty-seven blade bending and torsional moment strain gauge measurements (distributed amongst the four blades), one rotating pitch-link measurement, one blade root pitch angle measurement, three stationary control system measurements and standard wind tunnel operating condition measurements.

German-Dutch Wind Tunnel (DNW) Tests

The wind tunnel test program in the DNW was performed with the DLR's Modular Wind tunnel Model (MWM). Reference 16 describes the capabilities of the MWM in detail.

The complete wind tunnel model consisted of a 40% scaled rotor and fuselage. Although a tail rotor was not installed, the drag of the tail rotor hub and shaft were roughly simulated by a simple cylinder. Both the rotor and the fuselage were each equipped with a 6-component balance. Rotor torque was measured by a torque meter and by the rotor balance. Since the rotor model allowed for the measurement of mast bending in the rotating axis frame and the rolling and pitching moment in the fixed axis frame, correlation between these signals was important. Therefore, one requirement of the test program in the DNW had been to trim the rotor to the 1p mast moments (sine and cosine) and to the steady rotor balance roll and pitch moments. The influence on rotor performance (i.e., lift, drag and power) was not significant for these different trim procedures.

The rotor blades were equipped with flap, lead-lag, and torsion sensors as shown in Table 1.

Table 1. Model-scale rotor blade instrumentation.

Blade No.	Flap	Lag	Torsion
reference	14	12	8
2	2	1	-
3	4	2	1
4	4	2	1

The wind tunnel program in the DNW was tailored to five different tasks:

- 1) Correlation with flight and 40- by 80-Foot Wind Tunnel tests;

Sections tested: 6x6m closed, 8x6m closed, 8x6m open, 9.5x9.5m closed

- 2) Rotor trim to power from flight test;

Sections tested: 6x6m closed, 8x6m closed, 8x6m 12% slotted, 8x6m open, 9.5x9.5m closed

- 3) Minimized flap bending moment trim for zero α_{shaft} , correlation with 40- by 80-Foot Wind Tunnel tests;

Sections tested: 6x6m closed, 8x6m closed, 8x6m 12% slotted, 8x6m open, 9.5x9.5m closed

- 4) Hover tests, correlation with flight tests and 40- by 80-Foot Wind Tunnel tests;

Sections tested: 6x6m closed, 8x6m closed, 8x6m open

- 5) Derivatives, correlation with 40- by 80-Foot Wind Tunnel tests;

Sections tested: 6x6m closed, 8x6m closed, 8x6m open, 9.5x9.5m closed (one speed only)

Tests with minimized flap bending trim at zero shaft angle (task 3) were conducted to identify trim differences between the RTA in the Ames 40- by 80-Foot Wind Tunnel test section and the scaled model in the DNW. Since the model control is well defined, data correlation between both configurations requires no interpolation.

The hover tests (task 4) were performed at -20° rotor shaft angle in the closed test sections and at 0° in the open test section.

The derivative measurements in task 5 are an essential tool if interpolation is necessary between measured results. Since the derivative elements (e.g., $\Delta C_T / \Delta \alpha$) are assumed to be linear in a small α -range only, the use of derivatives for extrapolation is often not accurate enough.

The most important parameters (e.g., thrust, rotor speed, etc.) were controlled in non-dimensional form so that the density influence was considered.

In all but the open test section, DNW personnel acquired wall pressure measurements using 92 pressure sensors. The sensors were installed along the floor (3 rows), along the side walls (2 rows each), and along the ceiling (3 rows). Preliminary signal analysis of the pressure sensors shows that the flow has strong gradients and has no symmetry. An in-depth signal analysis has not been performed yet.

CORRECTION METHODS

From early rotor investigations in wind tunnels it is known that wind tunnel measurements cannot directly be applied to free-flight conditions. Rotor reactions in the wind tunnel depend on various parameters such as:

- type of the test section (open, closed, slotted or closed on bottom only)
- shape of the test section (rectangular, square, elliptic, etc.)
- dimensions of the wind tunnel test section with respect to the rotor size
- position of the model rotor regarding distance to the wall (eccentricity)
- rotor disk loading, dynamic pressure, and wake skew angle

Additionally, the effects of tunnel blockage due to the rotor and support system and flow breakdown due to the impingement of the rotor downwash on the tunnel floor in the low speed regime also affect rotor loads and performance (e.g., power) as can be seen in Figs. 6-7.

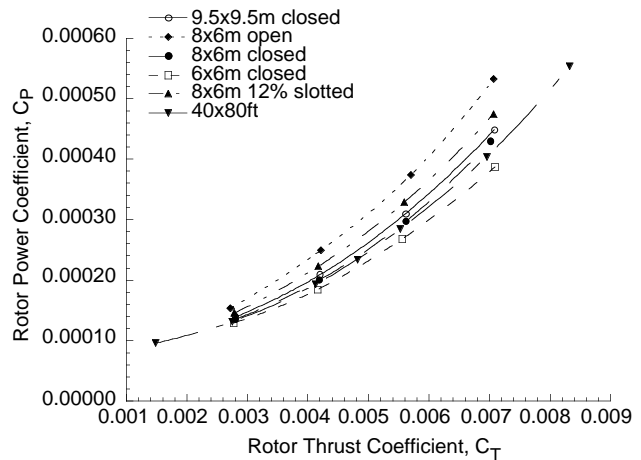


Figure 6. Rotor power as a function of rotor thrust with smooth flow conditions, $\mu = 0.07$, $\alpha_s = 0^\circ$.

Figure 6 shows a clear difference in rotor power between the open and closed test sections where smooth flow in the tunnel exists. This difference becomes small or even vanishes for conditions where flow breakdown exists as shown in Fig. 7. Therefore, wall correction methods are not applicable for conditions of flow breakdown.

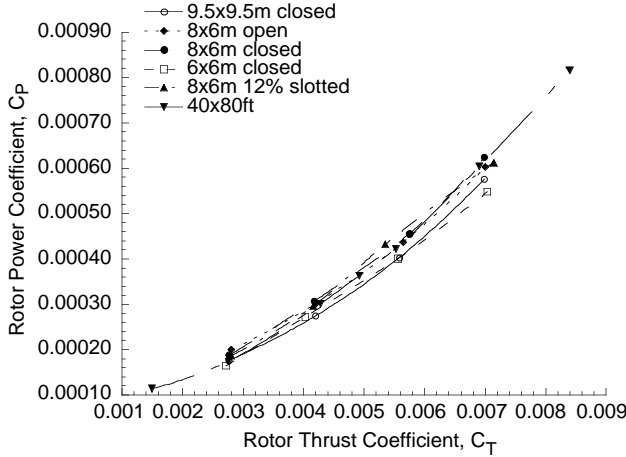


Figure 7. Rotor power as a function of rotor thrust with flow breakdown conditions, $\mu = 0.023$, $\alpha_s = 0^\circ$.

Corrections For Wall Interference

Wind tunnel wall induced interference can partly be eliminated by applying angle-of-attack corrections to the rotor shaft. Open test sections also require corrections, but of opposite sign to that of closed test sections.

To determine the direction of the angle-of-attack correction, one must imagine that the rotor flow is deflected by the test section ceiling which sharply turns the inflow. The test section floor changes the direction of the downwash, while the side walls have an impact on the rotation of the rotor flow. All can influence the local angle-of-attack due to inflow along the blade span.

Due to the change in inflow caused by the test section ceiling the rotor needs a more negative incidence to compensate for this effect. This is opposite to that for an open test section.

Glauert Correction Methodology

Glauert was the first to investigate in detail wind tunnel wall induced effects on wings. The Glauert correction is considered to be the classical or conventional wall correction method for fixed wing testing in a wind tunnel. The average downwash or induced angle correction is in the form

$$\Delta\alpha = \left[\frac{\delta_w A_{\text{wing}}}{A_{\text{TS}}} \right] c_L \quad (1)$$

where A_{wing} is the wing area, A_{TS} is the test section area and δ_w is the boundary correction factor. The boundary correction factor, δ_w is dependent on the test section shape, the ratio of the wing span to tunnel width and the position of the wing in the test section. A comprehensive collection of boundary correction factors for various test section shapes can be found in Ref. 2.

Assuming lift L_{wing} is equivalent to the rotor thrust T , but

$$L_{\text{wing}} = f(V) \quad \text{and} \quad T = f(v_{\text{tip}}),$$

c_L of Eq. (1) can be replaced by c_T using

$$c_L \equiv c_T \frac{v_{\text{tip}}^2}{V^2} \quad (2)$$

With

$$\mu = \frac{V}{v_{\text{tip}}}$$

Eq. (1) becomes

$$\Delta\alpha = \left[\frac{2 \delta_w c_T A_{\text{ro}}}{\mu^2 A_{\text{TS}}} \right] \frac{180}{\pi} \quad [\text{deg}] \quad (3)$$

and

$$\Delta\alpha = \alpha_{\text{FT}} - \alpha_{\text{WT}} \quad (4)$$

Note that Eq. (3) has a factor of 2 due to the fact that δ_w for wings refers to the wing span and thus $2R$ for rotors.

The boundary correction factors used in this paper are found in Table 2. Also shown in Table 2 are the corresponding values for rotor diameter to wind tunnel test section width. The boundary correction factors for the DNW test sections were determined from the figures found in Ref. 2. The boundary correction factor for the 40- by 80-Foot Wind Tunnel was determined from a figure found in Ref. 17.

In addition, δ_w can also be found by using more comprehensive flow correction theories or by experiment as will be discussed later.

Table 2. Wall correction factors δ_W from Ref. 2 and 17.

Test Section	D/W	δ_W
DNW 6x6m closed	0.667	0.160
DNW 8x6m closed	0.500	0.119
DNW 9.5x9.5m closed	0.421	0.145
DNW 8x6m open	0.500	-0.158
Ames 40x80ft	0.403	0.112

For completeness it should be mentioned that a similar closed form equation can be found in Ref. 10 as shown below

$$\Delta\alpha = F \tan^{-1} \left(\frac{c_T \cos \alpha_{FT}}{2 \mu^2 - c_T \sin \alpha_{FT}} \right) \quad (5)$$

Without substantial lack on accuracy the above equation can be re-written

$$\Delta\alpha = F \frac{c_T}{2 \mu^2} \quad (6)$$

The factor 2 in Eq. (6) comes from the air density that is often given as ρ instead of $\rho/2$ when thrust is written in the non-dimensional form.

From Eqs. (3) and (6) one gets the correction factor F

$$F = 4 \delta_w \frac{A_{ro}}{A_{TS}} \quad (7)$$

Heyson and Brooks Correction Methodologies

To determine boundary correction factors (δ_W) or for local angle-of-attack corrections along the blade span, Heyson's approach is widely used. The Heyson approach is based on 'potential theory' assumptions (Refs. 3-6). This method can be applied to rectangular test sections that can be closed, open, or closed on the bottom only. The resulting angle-of-attack and dynamic pressure corrections are dependent on various parameters such as rotor to test section width, width to height ratio, tunnel speed, rotor radius, hub eccentricity, rotor rotational speed

and thrust. The FORTRAN programs of Heyson are found in Ref. 4.

When a disagreement was found between calculated correction factors as determined by the Langley modified version of the Heyson program, and the boundary correction factors found in Ref. 2, it was determined that the Langley version contained a coding error. As a result of this disagreement and the desire to determine a detail mapping of wind tunnel corrections over the region of the rotor disk, Brooks derived a new correction method (Refs. 12-13). Results from this code have been validated by comparing correction values with those from a variety of published benchmark correction cases.

The approach used by Brooks is similar to that used by Heyson, however it is based on vortical rather than dipole wake distribution modeling. The Brooks code contains streamline curvature effects due to a lifting rotor in rectangular test sections. This code gives a spatial distribution of the correction, while the Heyson code gives only the correction in the rotor disk plane. Solid and wake blockage effects are not included in the Brooks code since it is assumed that in an open test section the stream is free to expand and in a closed test section the model size is much smaller than the cross-sectional area.

The Brooks code has been applied to all DNW test sections with the exception of the slotted walls. Because this paper deals only with rotor performance rather than local blade loads, results from Brooks code are used solely for the calculation of the global angle-of-attack correction, $\Delta\alpha$. Angle-of-attack corrections ($\Delta\alpha$'s) as calculated by the Brooks code are compared with the $\Delta\alpha$'s from Eq. (3) and δ_W 's from Table 2. Comparisons of the Glauert equation results with the results from the Brooks code are shown in Figs. 8-10. More detailed comparisons of each method are presented in the results section of the paper.

Figure 8 is a comparison of the angle-of-attack corrections for the Glauert equation and the Brooks code calculations as a function of rotor thrust at a fixed advance ratio ($\mu = 0.072$). For the 6x6m closed test section, the Glauert equation calculates a larger $\Delta\alpha$ -correction as a function of rotor thrust than the Brooks code calculations. Also, the difference in the $\Delta\alpha$ -corrections between the two methods increases with increasing thrust. Figure 9 is a comparison of the angle-of-attack corrections as a function of advance ratio for the 6x6m closed test section. The calculations shown in Fig. 9 are for a fixed value of rotor thrust ($c_T = 0.005$). The difference in the $\Delta\alpha$ -corrections between the two methods is greatest at the lowest speeds and the difference decreases as advance ratio is increased.

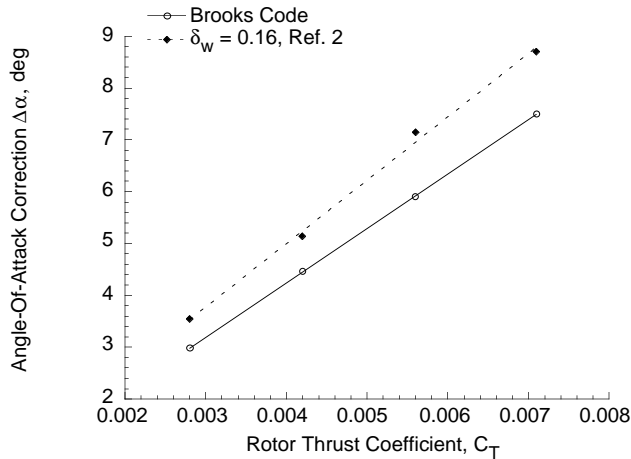


Figure 8. Correction angles as a function of rotor thrust from the Brooks code and Eq. (3), $\mu = 0.072$, 6x6m closed test section.

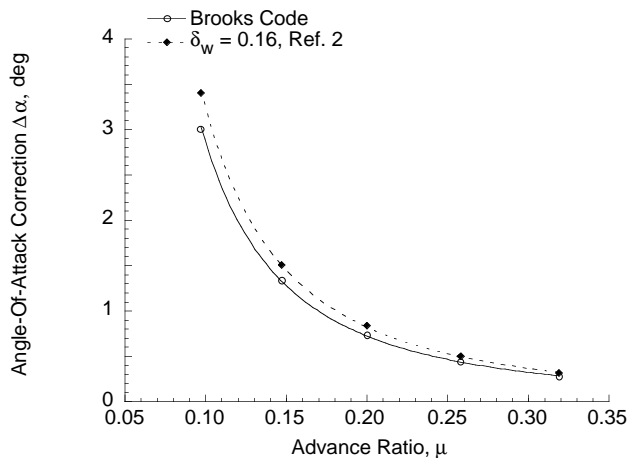


Figure 9. Correction angles as a function of advance ratio from the Brooks code and Eq. (3), $c_T = 0.005$, 6x6m closed test section.

Figure 10 is a comparison of the angle-of-attack corrections as a function of advance ratio for the 8x6m closed test section. The calculations shown in Fig. 10 are for a fixed value of rotor thrust ($c_T = 0.005$) similar to those shown in Fig. 9. Unlike Fig. 9, the difference in the $\Delta\alpha$ -corrections between the two methods is negligible over the whole speed range.

Figures 8-10 show that there can be differences in the calculated $\Delta\alpha$ -corrections between the Glauert formula and the Brooks code. At this point it is not known which method is more accurate. It may be that the boundary correction factor, δ_W for the 6x6m closed test section has to be re-determined. A new value for δ_W can be determined by feeding the $\Delta\alpha$ value from the Brooks code

into Eq. (3) as will be discussed in the next section of the paper.

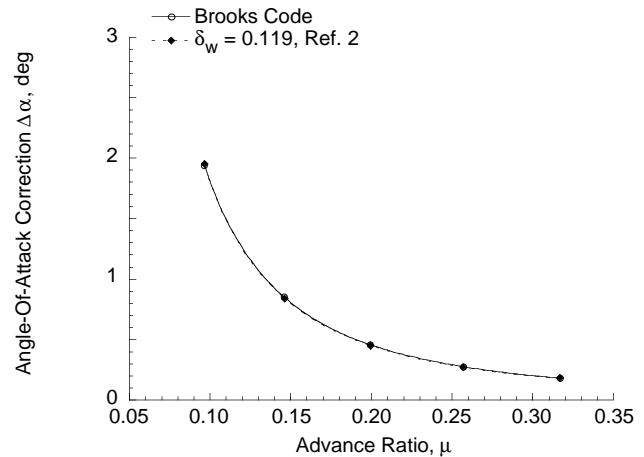


Figure 10. Correction angles as a function of advance ratio from the Brooks code and Eq. (3), $c_T = 0.005$, 8x6m closed test section.

Correction Factors Derived From The Brooks Code

The Brooks code $\Delta\alpha$ -results were fed back into Eq. (3) resulting in new boundary correction factors, δ_W as given in Table 3. The boundary correction factors in Table 3 can be applied to all c_T 's and all μ 's. This is important to know because it allows on-line global angle-of-attack correction within a test program. Using δ_W from Table 3, the differences between $\Delta\alpha$ from the Brooks code and the Glauert formula are negligible. Also shown in Table 3 are the corresponding values for rotor diameter to wind tunnel test section width.

Table 3. Boundary correction factors (δ_W) as determined by the Brooks code.

Test Section	D/W	δ_W
DNW 6x6m closed	0.667	0.1353
DNW 8x6m closed	0.500	0.1163
DNW 9.5x9.5m closed	0.421	0.1345
DNW 8x6m open	0.500	-0.1775
DNW 8x6m 12% slotted*	0.500	-0.0081

* δ_W determined from experiment

The boundary correction factor for the open test section given in Table 3 is related to an 8x6m effective test section size. Due to flow contraction, the effective tunnel dimensions may be somewhat smaller (e.g.,

7x5m). An exact value can hardly be given as it depends on the rotor condition (e.g., thrust) and its position with respect to the tunnel flow.

The wall correction factor for the 8x6m slotted wall test section is of high interest as it indicates that this test section needs only negligible $\Delta\alpha$ -corrections for rotor testing. This has been confirmed by fixed wing measurements. In addition, fixed wing measurements have indicated that α -corrections are necessary along the longitudinal axis of the model in the flow direction due to a longitudinal velocity gradient (Ref. 7). The negative sign of boundary correction factor (δ_W) shows that the slotted test section behaves more like an open section than a closed section.

Although the Brooks code is not applicable for the 8x6m slotted wall configuration, the boundary correction factor can be determined based on the measured results from the other test sections. Since it will be shown in a subsequent section of the paper that corrections for different test sections will collapse the power data onto a single curve, one can use this data to extrapolate to a test section that cannot be represented by the Brooks code if one assumes that these corrections are accurate. From the power difference between the corrected and uncorrected data one can determine the $\Delta\alpha$, and thus the δ_W with the help of Eq. (3). Strictly speaking, this procedure may only be used for identical test configurations.

Correction By Experiment

A prerequisite for the application of this method is that data from flight tests (e.g., rotor power and shaft angle) or from calculations are available and reliable. An applicable procedure is to trim the rotor in the wind tunnel to the measured rotor power from flight test by adjusting the shaft angle while maintaining constant c_L . This is the so-called trim to torque method (TtoT). This method allows for the determination of the difference between α_{FT} and α_{WT} and thus the angle-of-attack correction ($\Delta\alpha$) due to wall interference, assuming all other differences (i.e., scale, inflow, Reynolds No., ...) are negligible. The TtoT procedure is described in more detail in a later section of the paper.

Figures 11-13 show the variation in rotor power as a function of rotor shaft angle (α_{shaft}) for three different advance ratios. A dashed horizontal and vertical line represent the regression curve-fits of the rotor mast power and the flight test shaft angle (see also Fig. 4). The intersection between the rotor shaft angle in the wind tunnel and power from flight test is the corresponding free-flight condition. These figures show that with

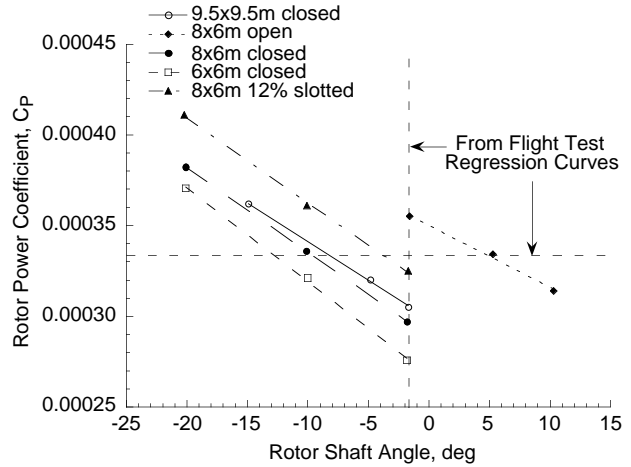


Figure 11. Rotor shaft power versus rotor shaft angle, $\mu = 0.056$, $c_L = c_{weight} = 0.005$.

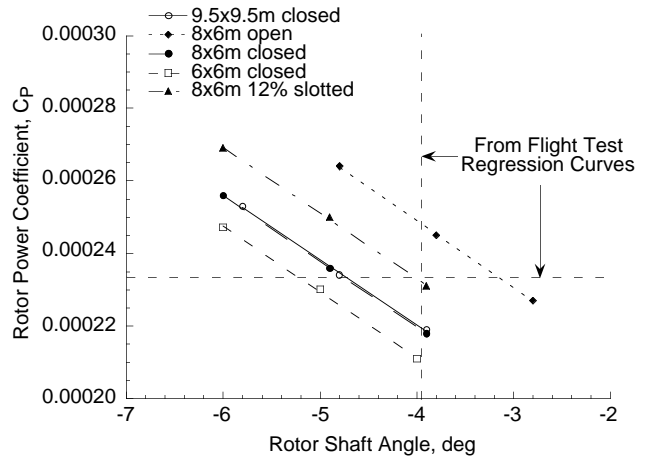


Figure 12. Rotor shaft power versus rotor shaft angle, $\mu = 0.172$, $c_L = c_{weight} = 0.005$.

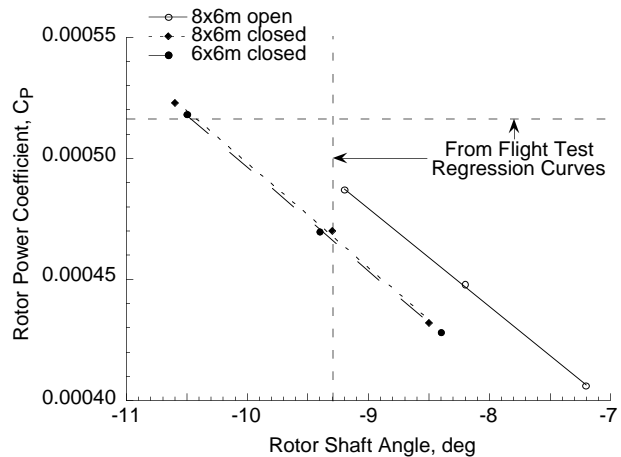


Figure 13. Rotor shaft power versus rotor shaft angle, $\mu = 0.32$, $c_L = c_{weight} = 0.005$.

increasing speed, the shaft angle difference between the intersection of the linear curve-fits and the flight test regression curve data becomes smaller between the different test sections. This is consistent with the wall correction theories where the wall induced angle-of-attack corrections reduce with increasing advance ratio, μ .

Corrections For Scaling Effects

Rotor loads and performance testing at model-scale requires careful design and manufacturing to simulate full-scale rotor behavior. In particular, the tip Mach number must be very close or equal to that of the full-scale rotor to capture the influence of compressibility on blade section loading. Blade per rev natural frequencies and Lock number must also be very close to provide similar coning and flapping. However, the Reynolds number for the scale model rotor will not match the full-scale values unless the model is run at higher pressures, either in a pressurized tunnel or by changing the working fluid of the tunnel.

Table 4. Comparison of full-scale (flight and wind tunnel) and model-scale rotors.

	model	Bo105	Factor*
Rotor Diameter [m]	4.0	9.82	s^{-1}
Rotor Speed [rpm]	1040	424	s
Blade Chord [m]	0.121	0.27	$0.91s$
Blade Twist [deg]	-8	-8	1
Tip Speed [m/s]	218	218	1
Solidity, σ	0.077	0.07	$0.91s$
Hub Precone Angle [deg]	2.5	2.5	1
Tip Mach No.	0.64	0.64	1
Re-No. at $r/R = 0.7$, $\times 10^{-6}$	1.26	2.82	2.24
Blade Profile	NACA 23012 mod.		

*Scale Factor $s = 2.456$

The 40% scale model Bo105 rotor tested in air at the DNW was designed according to the criteria stated above. Following conventional Mach scaling rules with both rotors running at a tip Mach number of 0.64, the full-scale and model-scale Reynolds numbers at 70% radius are 2.82 and 1.13 million respectively. Wind tunnel measurements conducted by Messerschmitt-Bölkow-Blohm GmbH (MBB) on a NACA 23012 airfoil have shown that this reduction in Reynolds number causes a decrease in $c_{L,max}$ from 1.58 to 1.35, or about 15%, and a decrease in the lift-curve slope of about 7.5%. Therefore, the airloads for the model blade would be low with respect to the inertial and elastic forces when compared to the

full-scale rotor. To compensate for this relative decrease in airloads at model-scale, the blade chord was increased by 10%. The influence of this increase in the model-scale chord is assessed below. Important rotor parameters and the resulting scale factors for the full-scale and model-scale rotors are given in Table 4. The influence of Reynolds number on rotor performance for model-scale rotor testing was addressed in Ref. 18. In Ref. 18 it was shown that the non-dimensional power consumption for a conventionally Mach scaled model rotor was higher than a full-scale rotor under the same conditions. From Ref. 18,

$$\Delta c_{P_0} = c_{P_{0,FS}} - c_{P_{0,mo}} \quad (8)$$

$$\Delta c_{P_0} = \frac{\sigma \Delta c_{d_0}}{8} (1 + 4.6 \mu^2) \quad (9)$$

$$\frac{c_{d_{0,FS}}}{c_{d_{0,mo}}} = \left(\frac{Re_{FS}}{Re_{mo}} \right)^5 \quad (10)$$

Since $Re_{mo} < Re_{FS}$ and from Eq. (10) is

$$c_{d_{0,mo}} > c_{d_{0,FS}}$$

From (8) and (9)

$$\Delta c_{d_0} < 0 \quad \text{and} \quad \Delta c_{P_0} < 0$$

Therefore

$$c_{P_{0,FS}} < c_{P_{0,mo}}$$

This was shown in Ref. 18, as an offset in the power coefficient versus thrust coefficient curves for a full-scale and a one-sixth scale CH-47D rotor in hover. A similar comparison for the rotors discussed here shows no offset in the power coefficient versus thrust coefficient curves between the full-scale Bo105 and the 40% scale model Bo105 with 10% increase in chord length. This may be seen in Fig. 14, where the full-scale rotor was tested in

the NASA Ames 40- by 80-Foot Wind Tunnel and the scale model rotor was tested in the DNW 8x6m open jet test section at the same tip Mach number. The good agreement in hover performance between the full- and model-scale rotors indicate that the increase in chord length for the model-scale rotor was an effective means of compensating for the Reynolds number difference, although differences due to profile roughness, compressibility effects, and the body or test stand were not investigated.

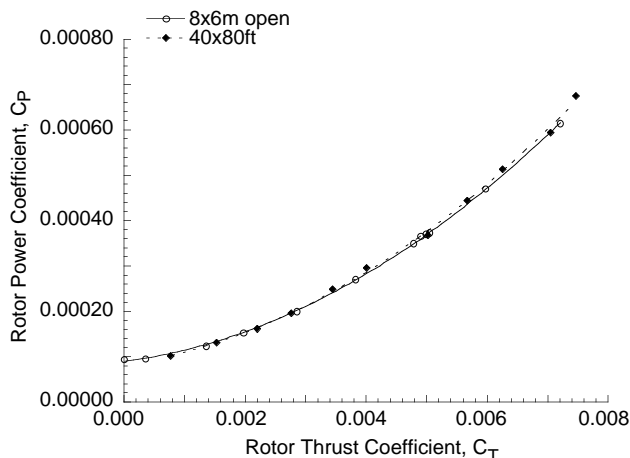


Figure 14. Comparison of full- and model-scale rotor power as a function of rotor thrust in hover.

ROTOR TRIM PROCEDURES

The goals of the 40% scale model DNW test were to measure rotor performance and blade loads on a model-scale rotor for the same conditions as were measured on a flight vehicle by the DLR, and to assess the wall corrections of the different test sections used at the DNW. To acquire wind tunnel data suitable for the first goal one must determine what is required to establish the same condition in the wind tunnel that existed for a particular flight point. Several different methods of adjusting the rotor control to achieve comparable trim conditions with the flight data were investigated.

During the full-scale Bo105 rotor test in the 40- by 80-Foot Wind Tunnel, three different trim conditions were established to compare with flight; minimized flapping trim, prescribed hub moment trim, and prescribed cyclic control angle trim (Ref. 15). All of these methods had in common the same rotor speed, shaft angle, rotor thrust, and tunnel speed. The prescribed hub moment trim requires the rotor operator to adjust the cyclic stick control until the steady hub pitch and roll moments agree with values measured from the flight aircraft. Minimized

flapping trim requires the rotor operator to adjust the cyclic stick control until the 1p flap moment in the flexure portion of the blade is a minimum (i.e., near zero). Cyclic control angle trim requires the rotor operator to adjust the cyclic stick control until the longitudinal and lateral cyclic displays agree with values that were measured on the flight aircraft. These different trim procedures cause the rotor tip-path-plane to deviate from one another resulting in different hub loads. Ideally, the prescribed hub moment trim and cyclic control angle trim methods would result in very similar conditions, however, the measurements shown in Ref. 15 show that the resulting hub loads were very different. Hub loads for minimized flapping trim were expected to be different from the other two trim procedures and this was the case.

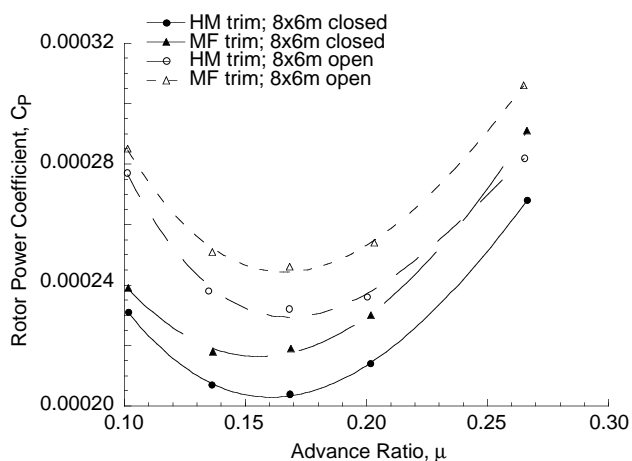


Figure 15. Comparison of rotor power as a function of advance ratio for minimized flapping (MF) and hub moment (HM) trim, $c_T = 0.005$.

Prescribed hub moment and minimized flapping trim were again used in the model-scale DNW test. Figure 15 compares the rotor power coefficient versus advance ratio for these two trim methods in the 8x6m closed and 8x6m open jet test sections in the DNW. Both the trim method and the test section are seen to have a strong influence on the rotor power. This shows the importance of choosing an accurate trim procedure. It further shows the significance of the test section used in the wind tunnel and demonstrates that some type of correction is required. The large differences shown in Fig. 15 along with the comparison with flight data shown in Ref. 15 indicate that minimized flapping trim is not suitable for comparisons with flight data. It does, however, provide a well-defined condition that will certainly be used in wind tunnel testing for a long time. The cyclic control angle trim has been investigated by the DLR and NASA and was found to produce large differences in hub loads when

compared to flight data, so it was not used in the DNW test.

The experimental test set-up in the DNW allowed additional methods of achieving the flight trim conditions. Because the rotor and the model-scale fuselage were mounted independently of each other on their own balance measuring device, the rotor and fuselage forces and moments could be measured independently. Independent measurements of rotor lift and fuselage lift provided the capability to trim the rotor lift to match the sum of the flight aircraft weight and the vertical force on the fuselage as defined by Eq. (11).

$$-c_{\text{Weight}} = c_{L,Ro} + c_{L,Fus} = c_L \quad (11)$$

This method removes the inaccuracy of assuming that rotor thrust is equal to aircraft weight, which is often used because $c_{L,Ro}$ and $c_{L,Fus}$ from flight are normally not known. At low speed the rotor induces a download on the fuselage producing a negative value of $c_{L,Fus}$ and at high speed the fuselage aerodynamics are likely to produce significant negative value of $c_{L,Fus}$. Trimming to lift as described above, assumes instead that the rotor wake and the model-scale fuselage behave in a similar manner aerodynamically to the flight aircraft.

Until now it had been assumed that the shaft angle measured in flight was accurate enough to establish comparable flight test trim conditions in the wind tunnel. Figure 15 clearly indicates that there is a significant influence on rotor power due to the wind tunnel test section. Therefore, a means of correcting for wall effects is required. An alternative approach to achieving the rotor trim of flight was evaluated for the first time in the DNW. The rotor was trimmed to rotor speed, rotor lift coefficient as defined by Eq. (11), tunnel speed, and hub pitch and roll moment coefficient. However, instead of trimming to the flight shaft angles, the shaft angle was adjusted until the measured shaft torque coefficient agreed with the flight measurement. Results for this trim to torque method (TtoT) are shown in Figs. 11-13. Since flight test data normally show a certain amount of scatter, three shaft angles were tested which bracket the flight power coefficient. From these tests, linear relationships of the change in the rotor power coefficient as a function of rotor shaft angle was established at each forward speed tested. These relationships and how they were used are discussed in a subsequent section of the paper.

Another approach to acquiring relationships similar to the trim to torque method, is to acquire data with small positive and negative perturbations in all the trim controls (e.g., V , α , $\theta_{0.7}$, θ_c , θ_s) around a baseline condition.

This derivative approach provides the information to correct the measured performance data for any parameter that turns out to be off the target trim value. However, it does require a significant investment in tunnel occupancy time to gather all the necessary derivatives. For the DNW test, the derivatives were taken after trimming to rotor speed, shaft angle, rotor thrust coefficient, tunnel speed, and hub pitch and roll moment coefficient. The results are more or less linear relationships between the control vector elements and the hub load vectors.

Since only the differences are of interest one can write

$$\underline{\Delta F} = \underline{D} * \underline{\Delta C} ,$$

where each element of matrix \underline{D} gives the slope of load vector \underline{F} and control vector \underline{C} .

The differences between the closed and open test section are clearly seen in the derivative data. The derivatives appear linear with advance ratio within the scatter of the data.

Representative results are shown in Figs. 16-18, where the change in thrust due to the change in three control vector elements are shown.

The derivative method is more general than the trim to torque method and was therefore applied for angle-of-attack corrections within the minimized flapping, zero shaft tilt test series. This will be shown in a later section of the paper.

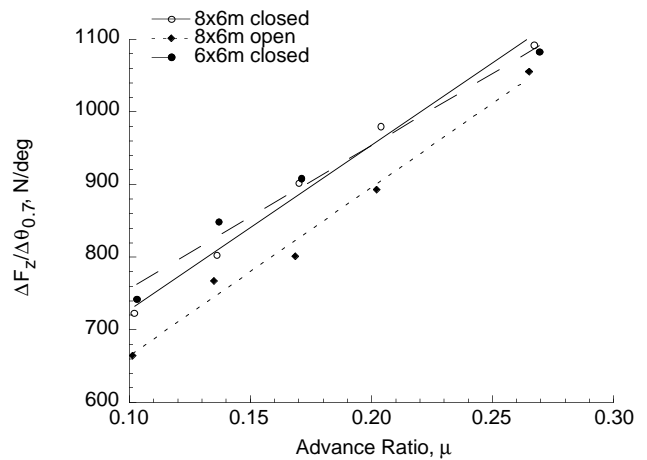


Figure 16. Collective derivative as a function of advance ratio for the 40% scale model rotor, hub moment trim.

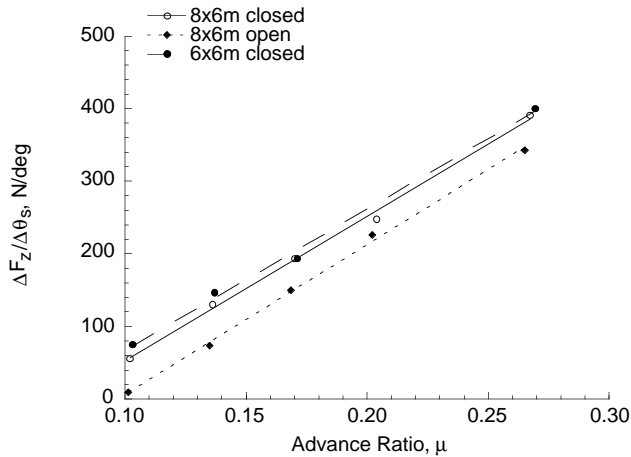


Figure 17. Longitudinal cyclic derivative as a function of advance ratio for the 40% scale model rotor, hub moment trim.

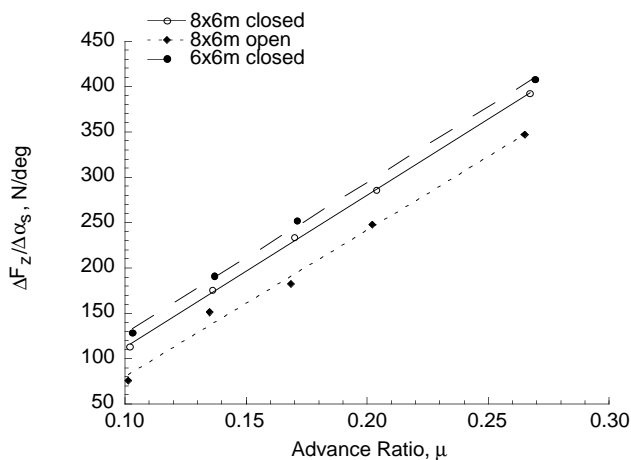


Figure 18. Shaft angle derivative as a function of advance ratio for the 40% scale model rotor, hub moment trim.

RESULTS

Trim Comparisons

Once the trim procedure has been established, experimental consideration determines whether these targets are simultaneously achieved. In this section, the ability to match hub moments and a comparison of the resulting 1p blade flapping moments are shown. The flight test trim target was established as steady level flight with minimum sideslip and no control input during data gathering. Steady hub moments were derived from harmonic analysis of the strain gauge signals on the rotating shaft.

In the last section several wind tunnel trim procedures were described. For the data shown in this section a single trim procedure was used for each wind tunnel. The full-scale test in the 40- by 80- Foot Wind Tunnel defined trim as matching rotor speed, shaft angle, tunnel velocity, rotor thrust equal to aircraft weight, hub pitch moment, and hub roll moment matching flight measurements. The hub moments were derived from balance measurements made below the rotor hub yet transferred to the hub center. The 40% scale-model test in the DNW defined trim as matching rotor speed, shaft angle, tunnel velocity, rotor lift equal to the sum of the aircraft weight and the vertical force on the scale model fuselage, 1p cosine shaft bending, and 1p sine shaft bending matching flight measurements.

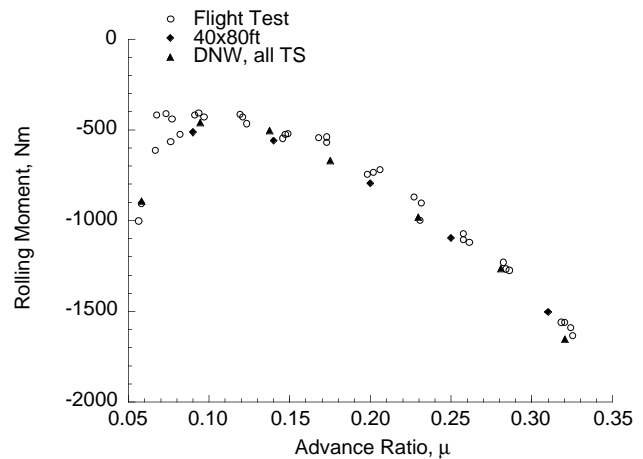


Figure 19. Comparison of measured hub roll moment as a function of advance ratio, $c_L = 0.005$.

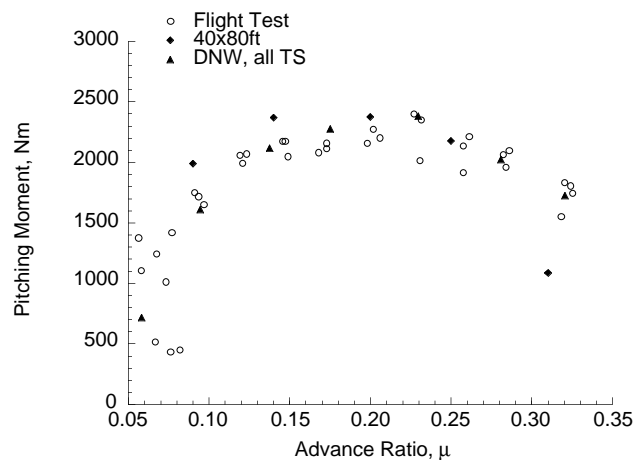


Figure 20. Comparison of measured hub pitch moment as a function of advance ratio, $c_L = 0.005$.

The ability to match the flight test targets may be seen in Figs. 19-20, where the 40% scale model rotor data have been scaled up for comparison. Figure 19 compares the rolling moment for these three tests. The flight data show relatively little scatter except at low forward speed where the speed indication is least accurate. In general the correlation is good. Figure 20 compares the pitching moment for these three tests. The pitching moment is of particular interest because it has a direct influence on the longitudinal tip-path-plane tilt, and since typical wind tunnel wall corrections impose an angle-of-attack correction, factors affecting tip-path-plane angle-of-attack are clearly important. Flight data shows more scatter for pitch moment than was seen for roll moment. This is most likely due to basic aircraft stability, atmospheric

unsteadiness, and slight deviations from steady level flight equilibrium. The 40- by 80- Foot Wind Tunnel data is slightly off the flight test target values at low speed and more significantly for the highest speed point where unsteadiness in the tunnel flow made it difficult to maintain a steady hub pitching moment. Unfortunately, there was only time for a single data point at each speed. It is expected that had more time been made available for gathering this data the agreement with pitch moments would be better.

Another way to assess the ability to which wind tunnel trim agrees with flight trim is to look at the resulting flapping moment along the span of the blades. Figure 21 shows the cosine component of the $1p$ flapping moment for the comparable highest speed points. The moment distributions look very similar except in the root section for the 40- by 80- Foot Wind Tunnel data. There are two things that can possibly explain this difference. Blade-to-blade dissimilarities as was shown in Ref. 15 can be one explanation for these differences. The other explanation to these differences is that the pitch moment does not agree well with the flight target value at this speed. Figure 22 shows the sine component of the $1p$ flapping moment with span for the comparable highest speed points. Better agreement is seen here over the entire span due to the good agreement in hub roll moments.

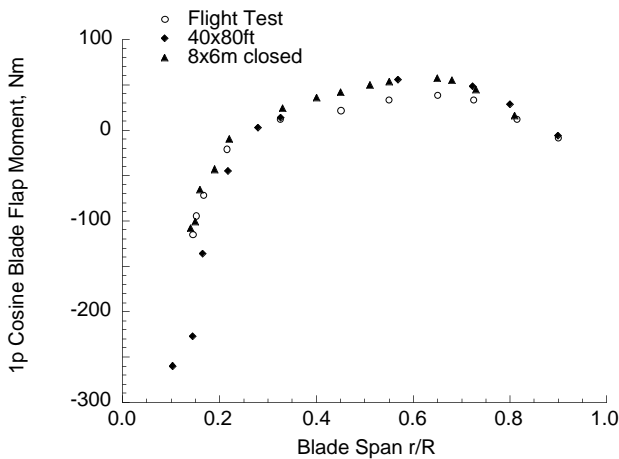


Figure 21. Longitudinal $1p$ flap moment distribution versus span, $c_L = 0.005$, $\mu = 0.32$.

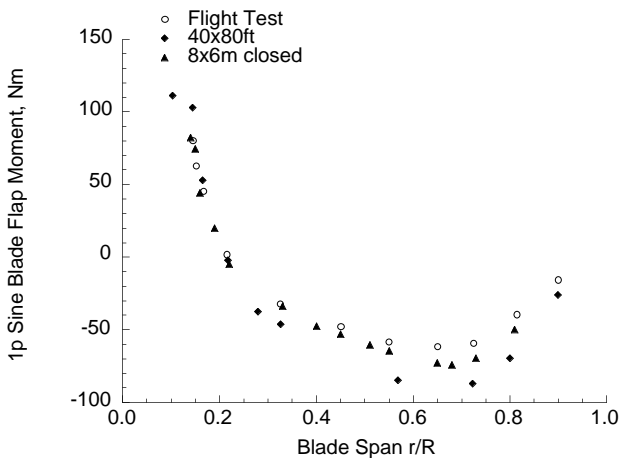


Figure 22. Lateral $1p$ flap moment distribution versus span, $c_L = 0.005$, $\mu = 0.32$.

Wall Induced Corrections

The primary focus of this paper is the presentation of the results from a series of systematic tests conducted in the DNW to identify the influence of tunnel walls on measured rotor performance and to evaluate the ability of existing wall correction methodologies to minimize facility dependent effects. To quantify the influence on the measured rotor performance of the various DNW test section configurations, two different approaches for rotor trim were used throughout this test program. Minimized flap bending moment trim was used to investigate the influence of wall induced effects on measured rotor performance as a function of rotor thrust and advance ratio. Prescribed hub moment trim, where the cyclic controls were adjusted until rotor hub moments matched values measured during previous flight testing were used to make comparisons with free-flight rotor performance in addition to investigating wall induced effects.

To quantify the influence of the tunnel walls on the measured rotor performance both as a function of forward speed and rotor thrust, a series of thrust sweeps utilizing a minimized flap moment trim was conducted at discrete forward speeds in each of the five different test section configurations. Due to forward speed limitations in some

of the test section configurations, not all test conditions were repeated. The influence of the tunnel test section on rotor power with minimized flap moment trim is clearly seen in Figs. 23-24. Figure 23 shows the rotor power as a function of rotor thrust at low speed ($\mu = 0.106$) for the five different test section configurations. Figure 24 shows the rotor power as a function of rotor thrust at high speed ($\mu = 0.251$) for the three test sections for which data is available. The data presented in Figs. 23-24 have not been corrected for the wall induced effects. The data shown in these two figures quantify the influence of the test section size on rotor power as measured in this test program. The trends with rotor thrust are very clear in both of these

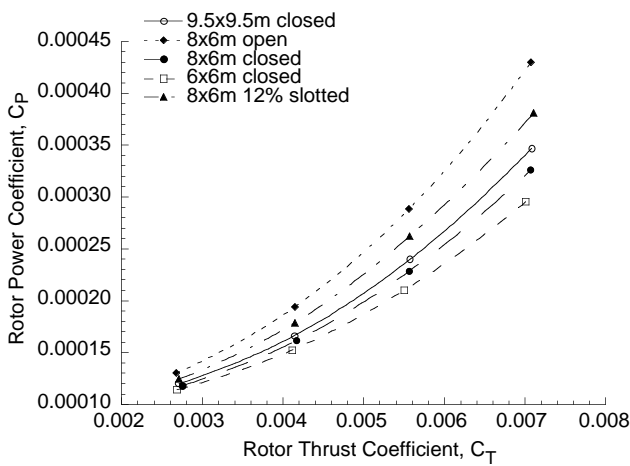


Figure 23. Comparison of rotor power as a function of rotor thrust for five different DNW test sections, minimized flap bending trim, $\mu = 0.106$, $\alpha_S = 0^\circ$.

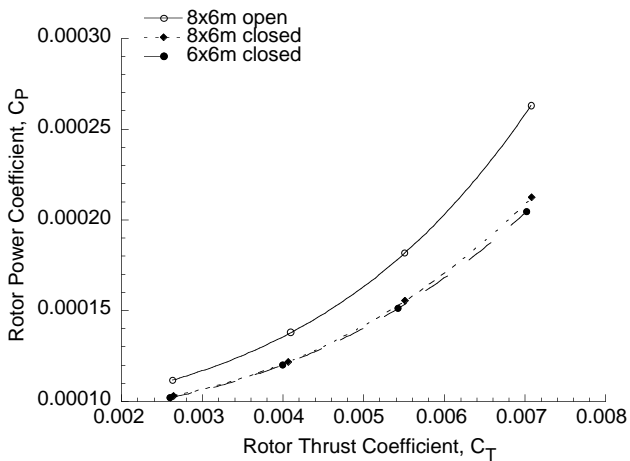


Figure 24. Comparison of rotor power as a function of rotor thrust for three different DNW test sections, minimized flap bending trim, $\mu = 0.251$, $\alpha_S = 0^\circ$.

figures. The data demonstrate that the influence of the tunnel walls increases as rotor thrust increases. It also shows that the measured power is lower with relatively smaller test sections. Both of these findings are consistent with existing wind tunnel wall correction methodologies. Differences between the 6x6m and the 8x6m closed test sections are much greater in Fig. 23 at low speed than they are in Fig. 24 at high speed. This trend is also consistent with existing wall correction theories.

The influence of the wall induced effects on rotor power as a function of tunnel speed is more clearly seen in Fig. 25. This figure shows rotor power as a function of tunnel speed with rotor thrust and hub moments adjusted to match flight test measurements. Data is presented for five different test section configurations. The data presented in Fig. 25 has not been corrected for the wall induced effects. The influence of the tunnel walls reduces as the tunnel speed increases. This is consistent with the measurements shown in Figs. 23-24 for minimized flap moment trim. These uncorrected measured data using prescribed hub moment trim in the different test sections will be referred to as 'baseline' measurements. Measurements with corrections for the influence of the tunnel walls or corrections to provide equivalent trim conditions will be compared to these baseline measurements.

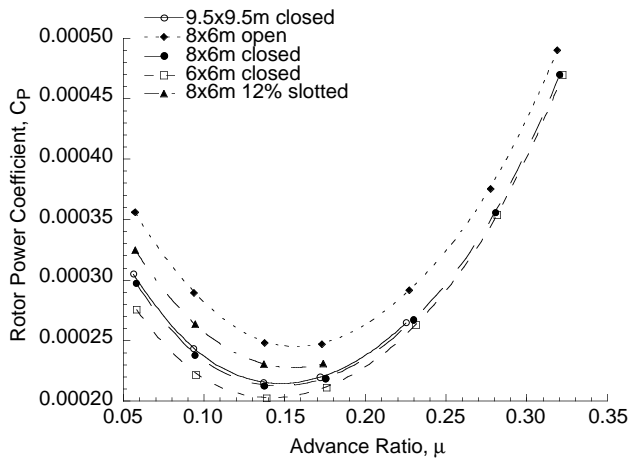


Figure 25. Comparison of rotor power as a function of advance ratio without wall corrections for five different DNW test sections with identical rotor trim conditions.

To quantify the influence of the tunnel walls on the measured rotor performance and to evaluate the existing wall correction methodologies upon completion of the DNW test program, a series of tests (trim to torque) was developed and utilized in each of the test section configurations. To allow for interpolation of the change

in rotor power as a function of rotor shaft angle, the rotor was trimmed with rotor thrust and hub moments adjusted to match flight test measurements at several rotor shaft angles around the measured flight test shaft angle. From these tests, a linear relationship of the change in the rotor power coefficient as a function of rotor shaft angle was established at each forward speed tested.

Two wall correction methodologies were selected for evaluation. The wall correction methodologies selected are the classical wall-correction method of Glauert (Glauert Eq.) and the Brooks computer code (Brooks Code). These

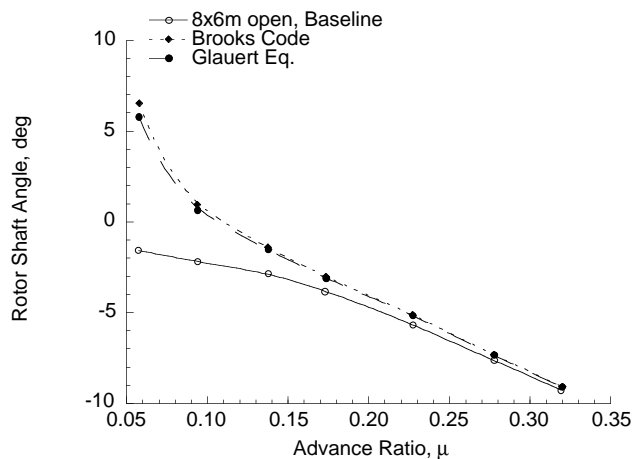


Figure 26. Comparison of baseline and wall corrected rotor shaft angle as a function of advance ratio in the 8x6m open jet test section.

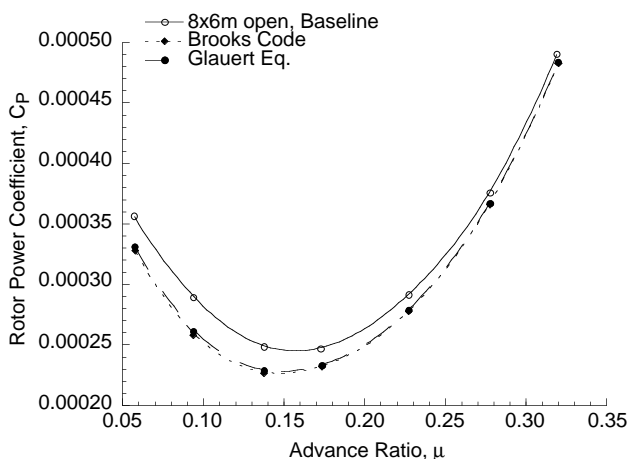


Figure 27. Comparison of baseline and wall corrected rotor power coefficient as a function of advance ratio in the 8x6m open jet test section.

methods are presented and discussed in a previous section of the paper. The results of these evaluations are presented in Figs. 26-31.

Comparison of baseline and corrected rotor shaft angle and rotor power coefficient data as a result of the two wall correction methodologies for the 8x6m open jet test section are shown in Figs. 26-27. Figure 26 presents a comparison of the wall corrected shaft angles (includes $\Delta\alpha$ -correction) with the baseline shaft angle as a function of advance ratio for the two wall correction methodologies. The rotor shaft angle requirements as determined by the Glauert equation and the Brooks computer code are very similar. For advance ratios greater than 0.15, the shaft angles are essentially identical. Small differences (less than one deg) in rotor shaft angle requirements were determined for advance ratios less than 0.15. The corresponding comparison of rotor power coefficient for each of the correction methodologies with the baseline as a function of advance ratio is shown in Fig. 27. Using the $\Delta\alpha$ -correction's from Fig. 26, both methodologies result in nearly the same rotor power over the entire speed range with negligible differences at the lowest speeds.

Results for the 8x6m closed test section are shown in Figs. 28-29. Comparisons of the baseline wind tunnel shaft angle as a function of advance ratio with the wall corrected shaft angles are shown in Fig. 28. The Glauert equation and the Brooks computer code calculate nearly identical values for shaft angle over the entire speed range. Comparisons of the corresponding rotor power coefficients with advance ratio are shown in Fig. 29. Based on the nearly identical corrected shaft angle results shown in Fig. 28, it is not surprising that the rotor power is nearly identical over the entire speed range as shown in Fig. 29.

Comparison of the results for each of the four test sections using the same correction methodology in each is shown in Figs. 30-31. Results using the Brooks computer code correction method are shown in Fig. 30. Figure 31 presents the results for each test section using the Glauert equation correction method. The results for the 8x6m open and closed test sections shown in Figs. 30-31 are the same as those presented in Figs. 26-29 comparing the different correction methodologies in each test section. Although direct comparisons of the two correction methodologies for the 9.5x9.5m and 6x6m closed test sections are not shown in the paper, the shaft angle and rotor power coefficient results were found to be very similar to those shown in Figs. 26-29.

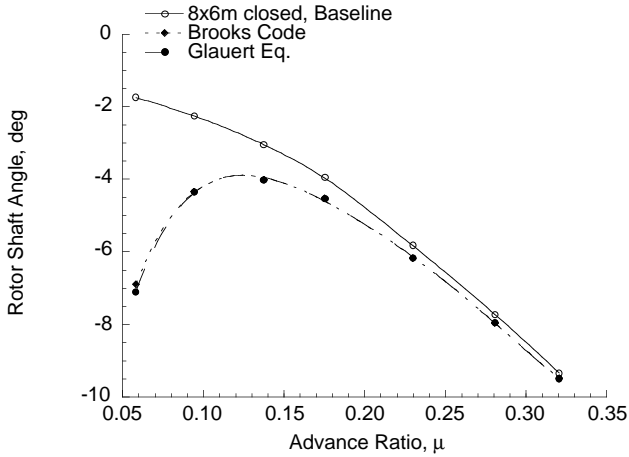


Figure 28. Comparison of baseline and wall corrected rotor shaft angle as a function of advance ratio in the 8x6m closed test section.

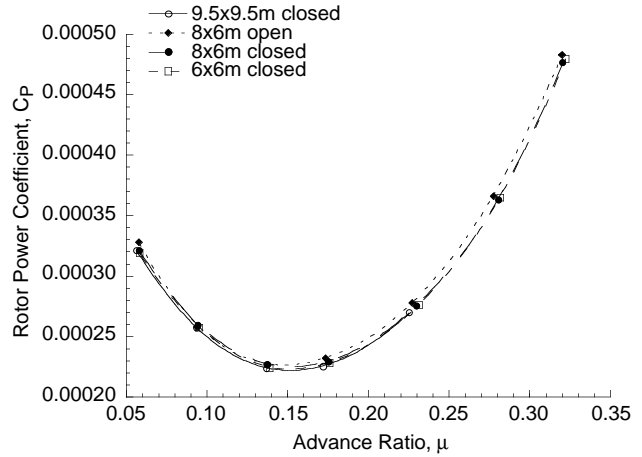


Figure 30. Comparison of wall corrected rotor power coefficient as a function of advance ratio using the Brooks code correction in four different DNW test sections.

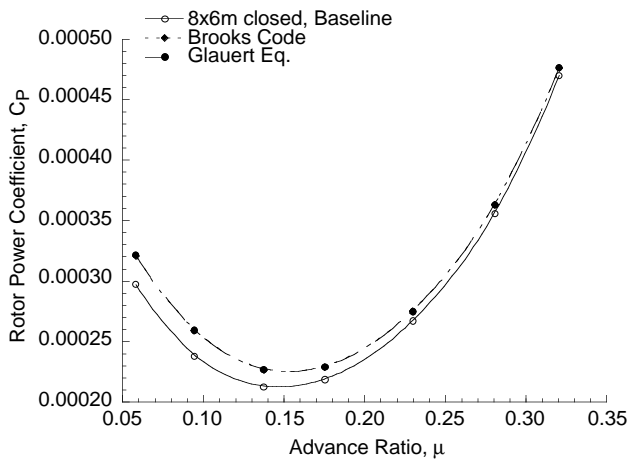


Figure 29. Comparison of baseline and wall corrected rotor power coefficient as a function of advance ratio in the 8x6m closed test section.

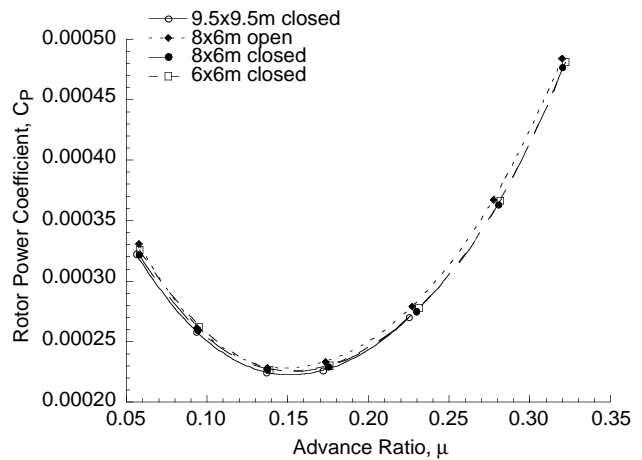


Figure 31. Comparison of wall corrected rotor power coefficient as a function of advance ratio using the Glauert equation correction in four different DNW test sections.

Results using the Brooks code are shown in Fig. 30 for each of the test sections. As seen in Fig. 30, the corrections based on the Brooks computer code have collapsed the data from the 9.5x9.5m, 8x6m and 6x6m closed test sections onto a single curve. For comparison purposes, refer to Fig. 25 that shows the uncorrected data and the distinct differences in the measured rotor power for each test section. The results for the 8x6m open jet test section indicate that perhaps not enough correction was made to this set of data relative to the other three test sections. Further review of this data set indicated that the resultant propulsive force was greater in the 8x6m open jet test section than the other test sections despite attempts to maintain consistent test conditions

throughout. The greater propulsive force in the 8x6m open jet test section resulted in higher measured rotor power.

The results of corrected rotor power using the Glauert equation correction method for each of the test sections are compared in Fig. 31. The comparisons shown in Fig. 31 are very similar to those shown in Fig. 30. This is to be expected based on the comparisons of correction methodologies shown previously where the Brooks computer code calculations and the Glauert equation corrections were nearly the same. As seen in Fig. 31, the Glauert equation correction has collapsed the data from the 9.5x9.5m, 8x6m and 6x6m closed test sections onto the

same curve. The results for the 8x6m open jet test section are very similar to that shown in Fig. 30 as is to be expected based on the comparisons shown in Fig. 27.

Propulsive Force Trim

The testing approach used to account for wall induced corrections as discussed in the previous section also resulted in linear relationships identifying the change in propulsive force with rotor shaft angle at each of the forward speeds tested. These relationships were determined so that a consistent propulsive force equilibrium for the rotor could be maintained during the evaluation of each of the wall correction methodologies. These relationships were used to correct the baseline values from each of the DNW test sections to the correct propulsive force representing the equivalent flat plate area of the Bo105 helicopter and subsequently the influence of the tunnel walls as defined by an angle-of-attack correction from each of the wall correction methodologies under evaluation. For the Bo105 helicopter (including rotor hub and shaft), the equivalent flat plate area is 1.33 m^2 (14.32 ft^2) as provided by Eurocopter Deutschland (ECD).

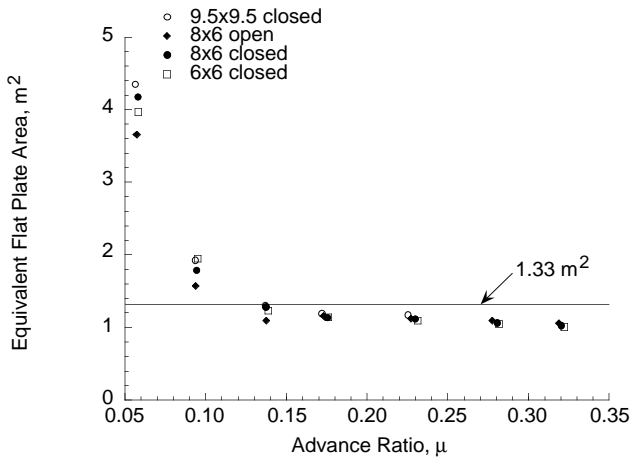


Figure 32. Comparison of equivalent flat plate areas as measured in each of the four DNW test sections with the ECD provided value of 1.33 m^2 .

Figure 32 presents a comparison of the equivalent flat plate areas as determined from data measured in each of the four DNW test sections as a result of trim conditions based on the shaft angle measurements from flight test and Eq. (11). Also shown on this figure is a horizontal reference line representing the equivalent flat plate area value of 1.33 m^2 as provided by ECD. For all advance ratios greater than 0.10, the equivalent flat plate area as determined in the wind tunnel is less than this value. The differences identified in this figure are the basis for the

propulsive force correction to the wind tunnel data using the linear relationships of the change in power and propulsive force with rotor shaft angle.

The first step in the analysis of this data was to correct the baseline wind tunnel data from each of the DNW test sections, in this case the rotor propulsive force to that which is determined by the equivalent flat plate area. By moving up or down the linear relationship of propulsive force as a function of rotor shaft angle at each forward speed, a corrected value of rotor shaft angle was established by matching the propulsive force to the prescribed flat plate area of 1.33 m^2 . This corrected value for rotor shaft angle primarily addresses the uncertainty and scatter of the flight test measurements. The other uncertainty that is not addressed directly in this analysis is the uncertainty in the measurement of the aircraft speed.

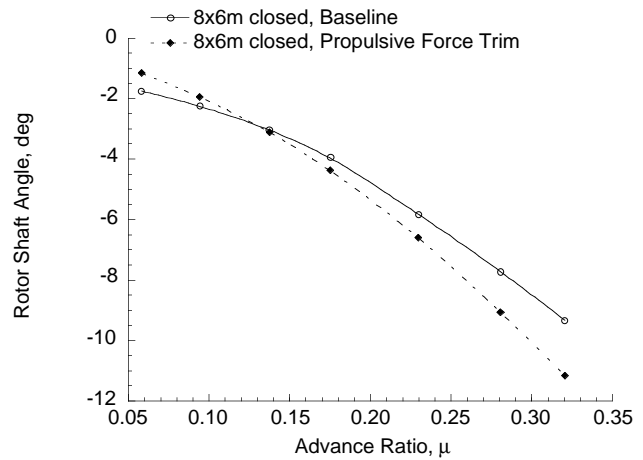


Figure 33. Comparison of baseline shaft angle with shaft angle for propulsive force trim in the wind tunnel as a function of advance ratio.

Figure 33 shows a representative comparison of the baseline wind tunnel rotor shaft angle (without wall induced corrections) as determined from flight test with the rotor shaft angle due to propulsive force corrections of the wind tunnel data as a function of advance ratio. This corrected rotor shaft angle value at each forward speed was then used to determine the corrected rotor power coefficient using the linear relationship of the change in rotor power coefficient as a function of rotor shaft angle. A comparison of corrected rotor power coefficient based on propulsive force trim (without wall induced corrections) with measured rotor power in the 8x6m closed test section based on rotor shaft angle from flight test as a function of advance ratio is shown in Fig. 34. Also shown on Fig. 34 is the measured rotor power data from flight test for three different speed sweeps as

discussed previously in this paper. The importance of propulsive force trim corrections to the measured wind tunnel data is evident in Fig. 34 at the higher advance ratios. Evaluations with different equivalent flat plate areas were also conducted. From these evaluations it appears that the value provided by ECD was indeed the most appropriate or representative value for these comparisons.

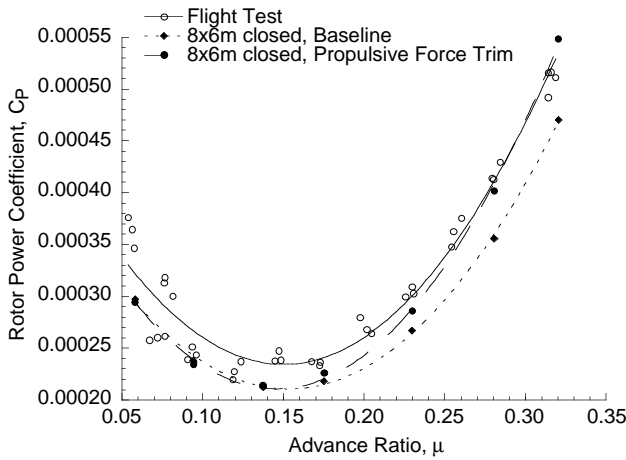


Figure 34. Comparison of baseline and propulsive force trim corrected rotor power coefficient in the wind tunnel as a function of advance ratio with flight test measurements.

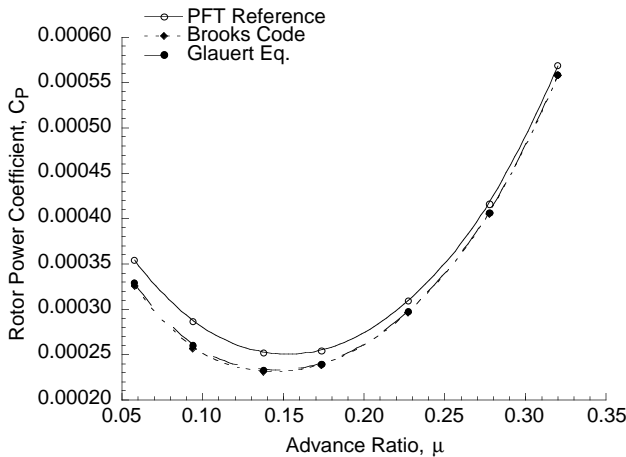


Figure 35. Comparison of propulsive force trim (PFT) reference and wall corrected rotor power coefficient as a function of advance ratio in the 8x6m open jet test section.

Results using the propulsive force trim analysis with and without wall corrections applied for the 8x6m open and closed test sections are shown in Figs. 35-36. Figure

37 compares the four different DNW test sections using the Brooks computer code correction method. All data presented have been corrected to an equivalent flat plate area of 1.33 m^2 (14.32 ft^2) before application of corrections for wall induced effects.

Comparison of propulsive force trim reference and corrected rotor power coefficient data as a result of the two wall correction methodologies for the 8x6m open jet test section is shown in Fig. 35. This figure may be compared with Fig. 27 to show that propulsive force trim has little influence on the final corrected rotor power coefficient results for $\mu < 0.25$. However, the wind tunnel wall corrected rotor power coefficient result for propulsive force trim is 15% greater at $\mu = 0.32$. As is to be expected from the results previously shown in Fig. 27, the corrected rotor power coefficients for the Glauert equation and the Brooks computer code methodologies are nearly identical.

Rotor power coefficient results for the 8x6m closed test section are shown in Fig. 36. Comparison of the propulsive force trim reference rotor power coefficient with the corrected rotor power coefficients based on the two wall correction methodologies as a function of advance ratio as shown in Fig. 36 is very similar to that shown in Fig. 29. As was shown in Fig. 29 and again in Fig. 36, the results using either wall correction method are virtually identical.

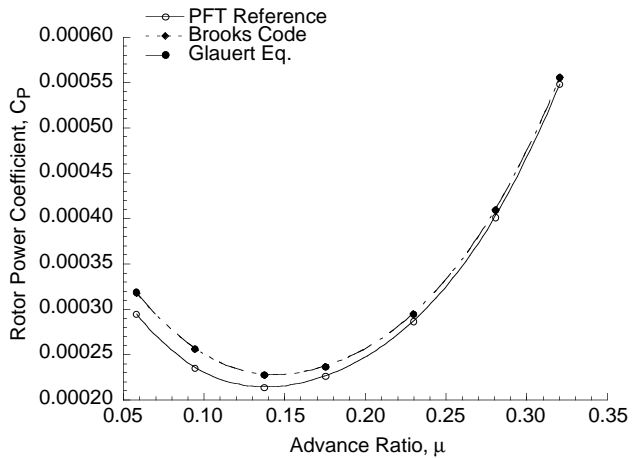


Figure 36. Comparison of propulsive force trim (PFT) reference and wall corrected rotor power coefficient as a function of advance ratio in the 8x6m closed test section.

Comparisons of the propulsive trim results for each of the four test sections using the Brooks computer code calculations are shown in Fig. 37. The comparisons are very similar to those shown in Fig. 30, except that the results for the 8x6m open jet test section have collapsed

onto essentially the same curve as that for the 8x6m and 6x6m closed test sections at the higher speeds. This improvement is largely due to the requirement for longitudinal force equilibrium between different test section data sets. At low speeds there still remain some differences as the influence of propulsive force on rotor power is small or negligible up to advance ratios of 0.15 as shown in Fig. 34. Remaining differences, although small, may indicate that not enough correction was identified by the correction methodology or there may be accuracy and repeatability limitations within the different data sets that has not yet been identified.

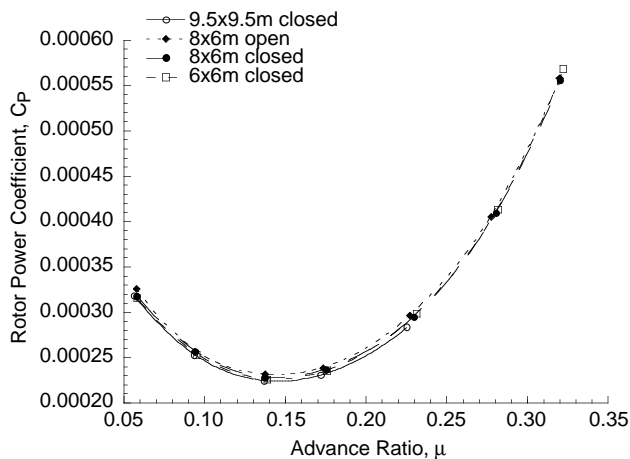


Figure 37. Comparison of wall corrected rotor power coefficient as a function of advance ratio using the Brooks code correction in four different DNW test sections, propulsive force trim.

Model-Scale/Full-Scale Flight Correlation

In addition to the test series developed to evaluate existing wall correction methodologies, another series of tests was conducted for direct comparison with data acquired in the NASA Ames Research Center 40- by 80-Foot Wind Tunnel. These data points were acquired, for the most part, at speeds other than those described in the previous series of tests and did not include variations in rotor shaft angle about a baseline value to determine the rotor power coefficient and propulsive force relationships. To apply the rotor power coefficient and propulsive force corrections to these data, relationships of the change in rotor power coefficient and propulsive force with rotor shaft angle as a function of advance ratio were determined. The relationships of rotor power coefficient and propulsive force with rotor shaft angle as functions of rotor thrust and advance ratio for the full-scale 40- by 80-Foot Wind Tunnel were determined from the comprehensive data base reported in Ref. 14. These

relationships were then used to correct the corresponding data for wall induced effects so that direct comparisons of model- and full-scale wind tunnel test and flight test data could be made as shown in Figs. 38-40. The wind tunnel data presented in Figs. 39-40 have been corrected to an equivalent flat plate area of 1.33 m^2 (14.32 ft^2).

Model- and full-scale results with and without corrections for propulsive force and wall induced effects for this series of tests are presented in Figs. 38-40. Although this series of tests was conducted in each of the four test sections, only the results for the 8x6m closed test section are shown for clarity. The results for the other test sections are very similar to the results shown previously in Figs. 26-31 and Figs. 35-37. Also shown in Figs. 38-40 is the corresponding flight test data previously shown in Fig. 34.

Comparisons of model- (8x6m closed) and full-scale (40x80ft) wind tunnel data without corrections for either propulsive force trim or wall induced effects are shown in Fig. 38. Measurements of rotor power from flight are also shown in Fig. 38. As seen in Fig. 38, the model- and full-scale rotor power data as measured in the wind tunnel for identical trim conditions compare reasonably well for advance ratios greater than 0.15. It is clear from Fig. 38 that both the model- and full-scale data do not compare well with the flight test data. Comparisons (not shown) of the baseline equivalent flat plate areas as measured in the wind tunnel for both the model- and full-scale rotors were very similar to the data shown previously in Fig. 32.

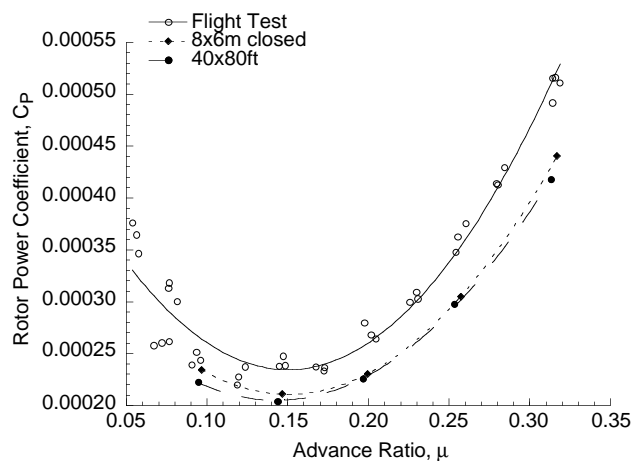


Figure 38. Comparison of model- and full-scale rotor power as a function of advance ratio without propulsive force trim or wall induced corrections with flight test measurements.

Model- and full-scale results that account for the propulsive force trim to an equivalent flat plate area of 1.33 m^2 (without wall induced corrections) are shown in Fig. 39 along with flight test measurements. Application of propulsive force corrections improved the correlation of the model- and full-scale wind tunnel data for advance ratios above 0.15, along with improvements in the correlation with flight test. Figure 39 clearly shows the importance of the propulsive force trim corrections in the correlation of these wind tunnel and flight test results.

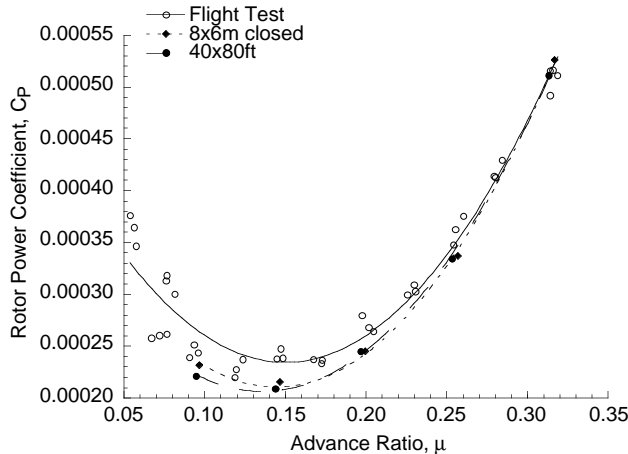


Figure 39. Comparison of model- and full-scale rotor power with flight test measurements as a function of advance ratio for propulsive force trim.

Rotor power results that include corrections for both propulsive force and wall induced effects from the 8x6m closed test section and the 40- by 80-Foot Wind Tunnel are compared with flight test measurements in Fig. 40. Both the model- and full-scale wind tunnel data were corrected using the Glauert equation correction methodology. The reason for selecting the Glauert equation correction method is that the Brooks code calculations are really only applicable for rectangular test section shapes. Because the 40- by 80-Foot Wind Tunnel is not rectangular, small errors in the analysis might be introduced with the use of the Brooks code to determine the angle-of-attack corrections. For advance ratios greater than 0.20, both the model- and full-scale results compare reasonably well with flight test. At the lower speeds, the model-scale results tend to follow more closely to the trends of the flight test, however there is sufficient scatter in the flight test data to be misleading in making this statement. Difficulties in maintaining a trimmed repeatable condition in flight at these low speeds makes it difficult to make any definitive statements regarding the correlation of either the model- or full-scale data with flight test measurements. Overall, the correlation of

model- and full-scale wind tunnel test data with flight test results is reasonably good.

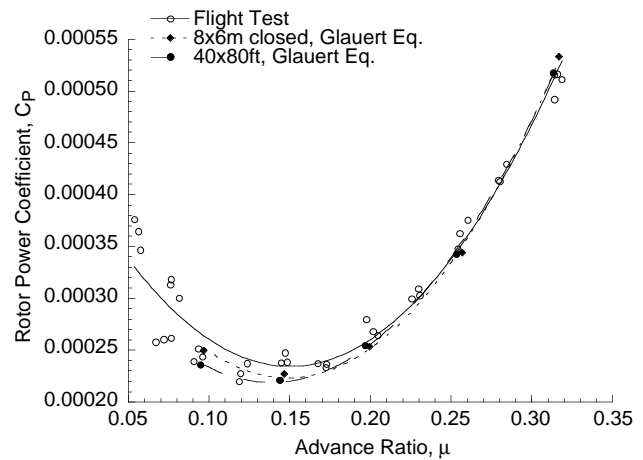


Figure 40. Comparison of model- and full-scale rotor power as a function of advance ratio with propulsive force trim and wall induced corrections with flight test measurements.

One possible explanation for the differences shown in Figs. 38-40 between the model- and full-scale results for advance ratios less than 0.15 is that the geometry of the two test sections is sufficiently different so as to affect the rotor downwash at the lower speeds. The 8x6m closed test section is a rectangular tunnel, while the 40- by 80-Foot Wind Tunnel is a closed test section with semicircular sides of 20 ft radius. As suggested in Ref. 9, the addition of fillets or in this case the influence of the semicircular sides may be reducing the allowable downwash or lift of the rotor. This is offered only as a possible explanation for these differences.

Model-Scale/Full-Scale Minimized Flapping Trim Correlation

As shown in the previous section, the propulsive force trim approach showed good correlation between flight and wind tunnel test rotor power. It is also possible to avoid the propulsive force issue and just look at comparing the measured performance of the two wind tunnel tests. Data gathered with minimized flapping trim and $\alpha_s = 0^\circ$, while not suitable for comparison with flight test, are especially suited for wind tunnel to wind tunnel comparisons. Figures 40-41 present a comparison between the full-scale rotor in the Ames 40- by 80-Foot Wind Tunnel and the 40% scaled model rotor in the DNW. Since the rotor trim is well-defined with this approach, results can be directly compared.

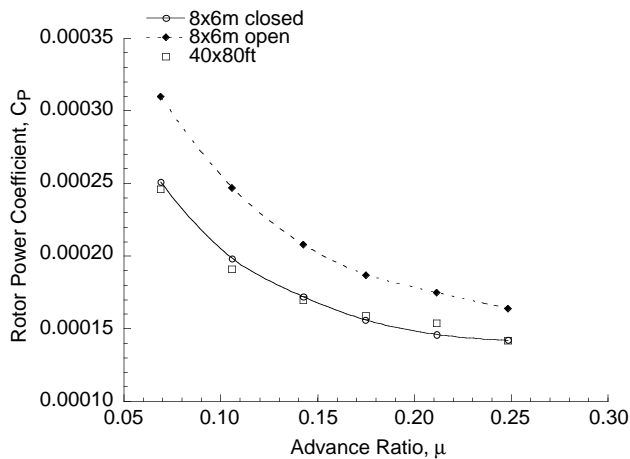


Figure 41. Comparison of model- and full-scale rotor power as a function of advance ratio for minimized flapping trim, $\alpha_s = 0^\circ$, $c_T = 0.005$.

Figure 41 shows full-scale rotor power in the 40- by 80-Foot Wind Tunnel with rotor power for the 40% scaled model rotor in the open and closed DNW test sections. The α_{TPP} is held constant as a result of the trim procedure for all advance ratios. Full- and model-scale data for the closed test sections are very similar indicating that the wall induced angle-of-attack corrections are of the same magnitude. The differences between the open and closed test sections also reduce as the tunnel speed increases. This is consistent with the results presented previously, indicating that the results are independent of α_{TPP} and in agreement with wall correction theory.

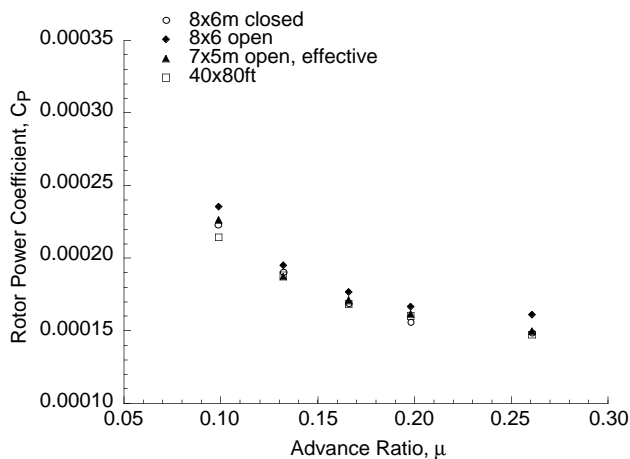


Figure 42. Comparison of model- and full-scale wall corrected rotor power as a function of advance ratio using the derivative correction method for minimized flapping trim, $\alpha_s = 0^\circ$, $c_T = 0.005$.

Comparison of the power curves from the 40- by 80-Foot Wind Tunnel and the 8x6m closed test section as shown in Fig. 41, indicate that the different model supports (RTA and 40% model-scale fuselage on the DNW sting) appear to have negligible influence on rotor power.

Figure 42 presents a comparison of the wall-corrected rotor power for the two wind tunnel tests. The angle-of-attack corrections were determined using the Brooks code, and the corresponding changes in power were determined using the derivative method. Since the speed derivatives (e.g., $\partial c_p / \partial V$) are non-linear, the derivative method is only accurate for speeds where derivatives were measured. Unfortunately, the experimental derivatives were not obtained at the advance ratio values shown in Fig. 41. Therefore it was necessary to use the least-squares curve fit in Fig. 41 to provide uncorrected values of rotor power at the advance ratio values for which derivatives were available. Linearity can be assumed for the α -derivative for small perturbations thus providing the power corrections required for the calculated $\Delta\alpha$'s.

Due to the uncertainty of the effective test section size of the 8x6m open test section (as previously discussed), the wall induced angle-of-attack corrections were also calculated for a 7x5m open test section. The smaller open test section size data collapses much better with the data from the 40- by 80-Foot Wind Tunnel and the 8x6m closed test sections.

CONCLUDING REMARKS

The influence of wind tunnel test section physical characteristics on measured rotor performance both as a function of rotor thrust and advance ratio were clearly shown.

The influence of wind tunnel wall induced interference on performance measurements can be compensated for by means of a global angle-of-attack correction. Both the Glauert equation and the Brooks computer code appear to provide adequate angle-of-attack corrections for rotor performance.

It was shown, that with proper trim procedures (i.e., hub moment and propulsive force trim) and corrections for wall induced interference effects, that it is possible to acquire model- and full-scale performance data in the wind tunnel that agrees well with flight measurements.

Differences in the model- and full-scale rotor supports used in the two wind tunnel tests reported here appears to have a negligible influence on the measured rotor power.

At nominal thrust values with the 40% scale model Bo105 rotor, the 8x6m slotted test section requires the smallest angle-of-attack corrections as compared to the other available DNW test sections.

REFERENCES

¹ Glauert, H., "The Interference on the Characteristics of an Airfoil in a Wind Tunnel of Rectangular Section," R & M 1459, 1932.

² Pope, Alan, and Harper, John J., Low-Speed Wind Tunnel Testing, John Wiley & Sons, Inc., 1966.

³ Heyson, H. H., "Use of Superposition in Digital Computers To Obtain Wind Tunnel Interference Factors for Arbitrary Configurations, With Particular Reference to V/STOL Models," NASA TR R-302, 1969.

⁴ Heyson, H. H., "FORTRAN Programs For Calculating Wind-Tunnel Boundary Interference," NASA TM X-1740, 1969.

⁵ Heyson, H. H., "Rapid Estimation Of Wind Tunnel Corrections With Applications To Wind Tunnel And Model Design," NASA TN D-6416.

⁶ Heyson, H. H., "Linearized Theory of Wind-Tunnel Jet-Boundary Corrections and Ground Effect for VTOL-STOL Aircraft," NASA TR R-124, 1962.

⁷ Garner, H. C., Rogers, E. W., Acum, W. E. A., and Maskell, E. C., "Subsonic Wind Tunnel Wall Corrections," AGARDograph 109, October 1966.

⁸ Rae, W. H. Jr., "Limits on Minimum-Speed V/STOL Wind Tunnel Tests," *Journal of Aircraft*, Vol. 4, (3), May-June 1967, pp. 249-254.

⁹ Rae, W. H. Jr., and Shindo, S., "An Experimental Investigation of Wind Tunnel Wall Corrections and Test Limits for V/STOL Wind-Tunnel Tests," U.S. Army Grant No. DA-ARO-31-124-G-809, Project No. 4506-E, AD-764 255, Dept. of Aeronautics and Astronautics, Univ. of Washington, July 1973.

¹⁰ Brooks, T. F., Jolly, J. R., and Marcolini, M. A., "Helicopter Main Rotor Noise," NASA TP 2825, August 1988.

¹¹ Shinoda, P. M., "Wall Interaction Effects For A Full-Scale Helicopter Rotor In The NASA Ames 80- By 120-Foot Wind Tunnel," Paper N° 20, AGARD 73rd Fluid Dynamics Panel Meeting and Symposium on Wall

Interference, Support Interference and Flow Field Measurements, Brussels, Belgium, October 1993.

¹² Brooks, T. F., and C. L. Burley, C. L., "A Wind Tunnel Wall Correction Model for Helicopters in Open, Closed, and Partially Open Rectangular Test Sections," NASA TM to be published August 1996.

¹³ Beaumier, P., Tung, C., Kube, R., Brooks, T. F. et al., "Effect of Higher Harmonic Control on Helicopter Rotor Blade-Vortex Interaction Noise: Prediction and Initial Validation," AGARD Symposium on Aerodynamic and Aeroacoustic of Rotorcraft; Berlin, Germany; October 11-13, 1994.

¹⁴ Peterson, R. L., "Full-Scale Hingeless Rotor Performance and Loads," NASA TM 110356, June 1995.

¹⁵ Peterson, R. L., Maier, T., Langer, H. J., and Tränapp, N., "Correlation of Wind Tunnel and Flight Test Results of a Full-Scale Hingeless Rotor," Proceedings of the American Helicopter Society Aeromechanics Specialist Conference, San Francisco, CA, January 1994.

¹⁶ Stephan, M., Klöppel, V., and Langer, H. -J., "A New Test Rig For Helicopter Testing," Proceedings of the Fourteenth European Rotorcraft Forum, Milan, Italy, 1988.

¹⁷ Johnson, W., and Silva, F., Rotor Data Reduction System User's Manual for the National Full-Scale Aerodynamics Complex NASA Ames Research Center, 1986.

¹⁸ Keys, C. N., Mc Veigh, M. A., Dadone, L., and Mc Hugh, F. J., "Considerations In The Estimation Of Full-Scale Rotor Performance From Model Rotor Test Data," Proceedings of the 39th Annual Forum of the American Helicopter Society, St. Louis, MO, May 1983.